

# **Geothermal Investigation of a 400 feet borehole near the University House on the UC Berkeley Campus**



**Kenichi Soga, Jiahui Yang, Kecheng Chen,  
James Wang, Yaobin Yang, Tianchen Xu,  
Andrew Yeskoo, Wonjun Cha, Shi-Hung Huang**

Department of Civil & Environmental Engineering  
University of California, Berkeley, CA

# **Contents**

Abstract	4
1 Introduction	5
2 Geological Conditions	7
2.1 Regional Geology	7
2.2 Seismic Setting	8
2.3 Site Geology of Berkeley Campus	9
2.3.1 Alluvial Deposit	10
2.3.2 Bedrock	11
2.3.3 Seismic Setting	11
2.3.4 Liquefaction	12
2.3.5 Groundwater	13
3 Borehole Investigation	15
3.1 Drilling Process	15
3.2 Soil Profile Description	17
3.3 Geophysical Logging	18
3.2.1 P-wave Velocity	18
3.2.2 S-wave Velocity	18
3.2.3 Televviewer Logging	18
3.3.4 Natural Gamma Logging	19
3.4 Comparison of Geophysical Log and Boring Log	19
4 Instrument Installation and Temperature Monitoring	21
4.1 Instrument Plan	21
4.2 Instrument Installation	22
4.3 Temperature Monitoring	23

4.3.1 Temperature Change during Grouting	23
4.3.2 Geothermal Gradient	25
5 Distributed Thermal Response Test	27
5.1 Installation of DFOS	27
5.2 Thermal Response Test Plan	28
5.2.1 Test Standards	28
5.2.2 Specific Procedures	28
5.3 First TRT Using OMNISENS (BOTDA)	29
5.3.1 GRTI TRT Rig Data	29
5.3.2 Inner DFOS Data	30
5.3.3 Outer DFOS Data	34
5.4 Second TRT Using ALICIA (BOTDR)	38
5.4.1 GRTI Data	38
5.4.2 Inner FOS Data	39
5.4.3 Outer DFOS Data	43
5.5 Geothermal Properties	46
6 Conclusion	50
7 Discussion and Future Works	51
Reference	53

## Abstract

The University of California, Berkeley, is building a clean electrified heating and cooling plant utilizing shallow geothermal to reduce greenhouse gas emissions. This report aims to investigate the geological conditions and provide the geothermal properties of the campus ground for evaluating the geothermal potential. A geological database of the Berkely campus was first established based on published geotechnical reports. It indicates the ground beneath the campus is primarily fill (0 – 3 ft thick), upper clay layer (20 – 40 ft thick), clayey sand with gravel (5 – 10 ft thick), and Franciscan Complex (very thick). To conduct the thermal response test (TRT), a 400-ft borehole with a diameter of 6 inches was drilled. The soil profile logged during drilling matches the geological database, and sheared zones are found at depths of 75 ft, 200 ft, 280 ft, and 330 ft. The drilling was followed by geophysical logging, including a caliper survey, a PS-wave Suspension survey, a televiewer survey, and a natural gamma logging survey. The result shows that the tilt of the borehole is less than 5° above the depth of 230 ft and increases to 12° at the bottom. The profiles of P-wave velocity, S-wave velocity, and natural gamma well recognize different types of soil/rock and depths of sheared zones. Before grouting, sensors including Distributed Temperature Sensor (DTS), Strain Fiber Optic Sensor, FBG piezometer, Vibrating Wire (VW) Piezometer, and Short-Period Geophone were attached to the U-pipe and installed inside the borehole. According to temperature sensors, the average geothermal gradient at the test site is 0.0136 °F/ft (24.79 °C/km). DFOS was also installed inside U-pipe to better monitor the temperature, and two distributed thermal response tests (DTRTs) were conducted. The average effective thermal conductivity is 1.38 Btu/hr-ft-°F for the first test and 1.35 Btu/hr-ft-°F for the second test, respectively. The analytical model developed by McDaniel et al. (2018) is used to extract geothermal properties from the DFOS data. For the sediment (above 30 ft) and the bedrock (30 – 250 ft) in the first test, the thermal conductivity is 6.2 Btu/hr-ft-°F and 1.4 Btu/hr-ft-°F, respectively, and the thermal diffusivity is 3.5 – 7.5 ft<sup>2</sup>/day and 0.8 – 1.2 ft<sup>2</sup>/day, respectively; for the sediment (above 30 ft) and the bedrock (30 – 250 ft) in the second test, the thermal conductivity is 6.2 Btu/hr-ft-°F and 1.4 Btu/hr-ft-°F, respectively, and the thermal diffusivity is 0.7 – 1.6 ft<sup>2</sup>/day and 1.1 – 1.8 ft<sup>2</sup>/day, respectively. Both tests indicate very low heat transfer efficiency below the depth of 250 ft, probably due to poor grouting quality. In the future, the FE method will be used to improve the estimate of geothermal properties and study the dissipation of residual heat into the ground during the temperature decay phase.

# 1 Introduction

The University of California has its Carbon Neutrality Initiative against global climate change to reduce greenhouse gas emissions (<http://sustainability.berkeley.edu/climate>). To meet this target, the campus plans to replace its aged natural gas cogeneration plant with a new 100% clean energy system for heating and cooling the whole campus. The system's core is a clean electrified heating and cooling plant, which can take advantage of shallow geothermal. Herein, the shallow ground is used as a heat source/sink, and a ground source heat pump (GSHP) system is applied to transfer heat between the system and the heat source/sink. The heat is extracted from the ground to heat buildings in winter, whereas it is injected into the ground to cool buildings in summer. By designing the GSHP system appropriately based on the campus's heating and cooling demands, the ground temperature can be balanced for the long-term operation of the system. Although the previous geothermal research by the authors has proven the potential of the shallow geothermal beneath the Berkeley campus through numerical simulations, in-situ tests are required to verify the simulation results and provide the geothermal properties of the campus ground for the detailed design of the proposed GSHP system.

A thermal response test (TRT) is an in-situ testing method to measure geothermal properties. As heated water circulates through the U-pipe installed and grouted inside a borehole, the supply and return temperatures at the ground surface are recorded. The geothermal properties are then estimated from the change in the temperature inside the U-pipe with time. The conventional TRT mainly uses the line-source or cylinder-source model that Carslaw and Jaeger (1959) developed to calculate thermal conductivity and borehole resistance. However, due to the infinite line source and constant heat rate assumptions, the vertical heat transfer and the effect of heating rate fluctuation are ignored.

In some cases, a numerical method is applied to consider the effect of borehole geometry, different properties of grout and ground, and varying heat transfer rates (Gehlin, 2002). It is usually combined with a parameter-estimation-based or inverse analysis method to evaluate the thermal conductivity value from TRT results (Sonder et al., 1999, Signorelli et al., 2007, Raymond et al., 2011). Numerical methods also make the analysis considering fracture flow and groundwater flow possible (Raymond et al., 2011). However, since only outlet and inlet temperatures are measured, the conventional TRT only extracts the thermal conductivity of the whole tested subsurface section.

The recent development of distributed fiber optic sensors makes the distributed thermal response test (DTRT) possible. Compared to the traditional TRT, DTRT can provide temperature change profiles along the depth during the tests and allow estimating the vertical distribution of geothermal properties. Analytical models (e.g., line-source model, cylinder-source model) can be applied to extract the geothermal properties in each sublayer from the temperature change profile measured by the distributed fiber optic sensors (Acuna et al., 2009, Fujii et al., 2009, Acuna 2013, Sakata et al., 2018, Beier et al., 2022). However, these analytical methods are based on the infinite line-source assumption and thus are not appropriate to be used in layered subsurface conditions. Numerical simulation combined with the parameter-estimation-based process can be applied to DTRT results to overcome this issue (e. g., Raymond et al. (2013), Liu et al. (2020), and Beier et al. (2021)).

This report aims to provide the geothermal properties of the campus ground to evaluate the geothermal potential. The specific tasks of the study include 1. collecting and analyzing the regional geological information; 2. building a digital geology database of the UC Berkeley campus; 3. drilling and installing a 400-ft investigation borehole with various sensors; 4. exploring the site geology through geophysical logging; 5. and conducting two distributed thermal response tests for the geothermal property evaluation of the campus ground.

## **2 Geological Conditions**

The Berkeley Campus is located in the San Francisco Bay Area. This chapter summarizes the regional geology and seismic setting of the San Francisco Bay Area. Based on the published geotechnical investigation reports, a geology database is built, and the site geology of the Berkeley campus is concluded.

### **2.1 Regional Geology**

The San Francisco Bay Area is in the subduction zone formed by the Pacific Plate, subducting beneath and creeping north against the North America Plate. Figure 2.1 gives an overview of the lithology distribution in the Bay Area. The Franciscan Complex/Assemblage, typically the accretionary wedge, was formed at this convergent boundary and became the main bedrock of the Bay Area. It is a tectonic mélange dominated by sandstone, greywacke, shale, and conglomerates. Other rock types, such as chert and serpentinite, can also be found. The Franciscan Complex mainly crops out on the eastern side of the San Andreas Fault and extends east to the Great Valley Sequence. Most of the Franciscan Complex was formed through the Jurassic age and then severely broken by the fault system before the deposition of soil sediments. Thus, the outcrops of the Franciscan Complex have different mechanical properties and degrees of erosion fracturing/weathering.

Five formations of the late Quaternary age compromised the primary soil sediments of the Bay Area (Trask & Rolston, 1951). From old to young, they are the Alameda formation, the San Antonio formation, the Posey, the Merritt, and the Bay Mud. Besides the Bay Mud, all other four formations have firm and stiff soil. The Bay Mud is notorious for its poor engineering properties, such as low strength and high compressibility. It is formed when eroded fine silt and clay particles carried in streams meet the still salty water in the San Francisco Bay and begin to settle. Figure 2.2 shows the distribution of the Bay Mud around San Francisco Bay.

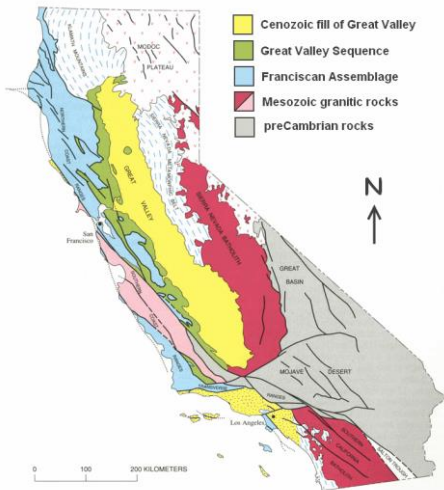


Figure 2.1 Lithology distribution of CA

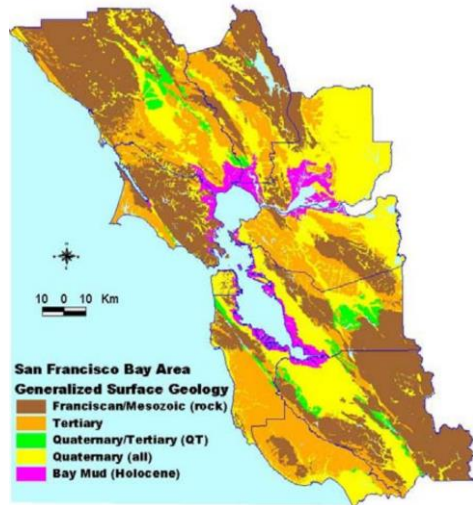


Figure 2.2 Distribution of Bay Mud (Silva et al. 2014)

## 2.2 Seismic Setting

Slow subducting and creeping of the Pacific plate against the North American Plate create the coastal ranges and the San Andreas fault system, which controls the seismic activity in the San Francisco Bay Area. The San Andreas Fault system is more than 600 miles long from Point Arena in the north to the Gulf of California in the south, and the local movement along the San Andreas totals roughly 1 inch (2.5 cm) every year. Figure 2.3 shows the distribution of the fault system, Alquist-Priolo Zones, and historical earthquake records. Large earthquakes threatening the San Francisco Bay Area can be blamed on the San Andreas fault system and its subsidiary faults, including the Hayward and Calaveras. USGS estimated a 72 % probability that at least one earthquake with a moment magnitude more significant than 6.7 will occur in the San Francisco Bay Area before 2044 (Field et al., 2015).

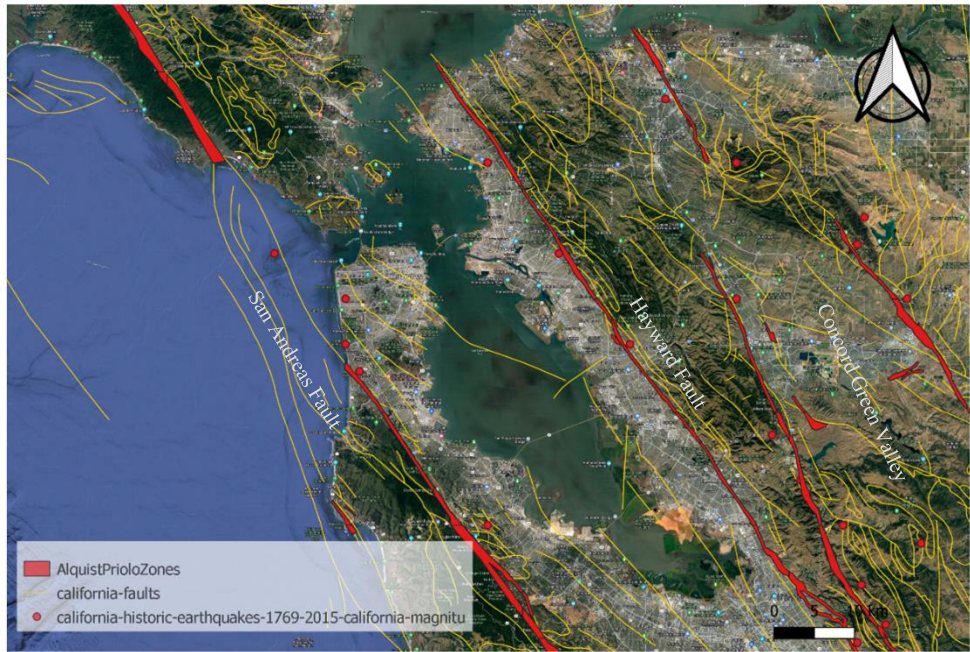


Figure 2.3 Distribution of Fault system in the San Francisco Bay Area (data from USGS)

## 2.3 Site Geology of Berkeley Campus

The UC Berkeley campus (37.87, -122.26) is located in downtown Berkeley at the foot of Berkley Hills, facing west to the San Francisco Bay. The campus is within the Berkley Hills block, one of the northwest-trending geomorphic divisions resulting from the tilting of the fault block. To better characterize the geologic condition of the Berkeley campus, a digital database of the campus geology was established based on the published geotechnical investigation reports since the 1950s, when the construction of the Berkeley Campus started. The borehole data was extracted and reorganized as input for the software LEAPFROG to build the campus 3-D geological model, as shown in Figure 2.4. The fault information from USGS is also added to show the fault system crossing the Berkeley campus and dividing the Franciscan Complex into different parts.

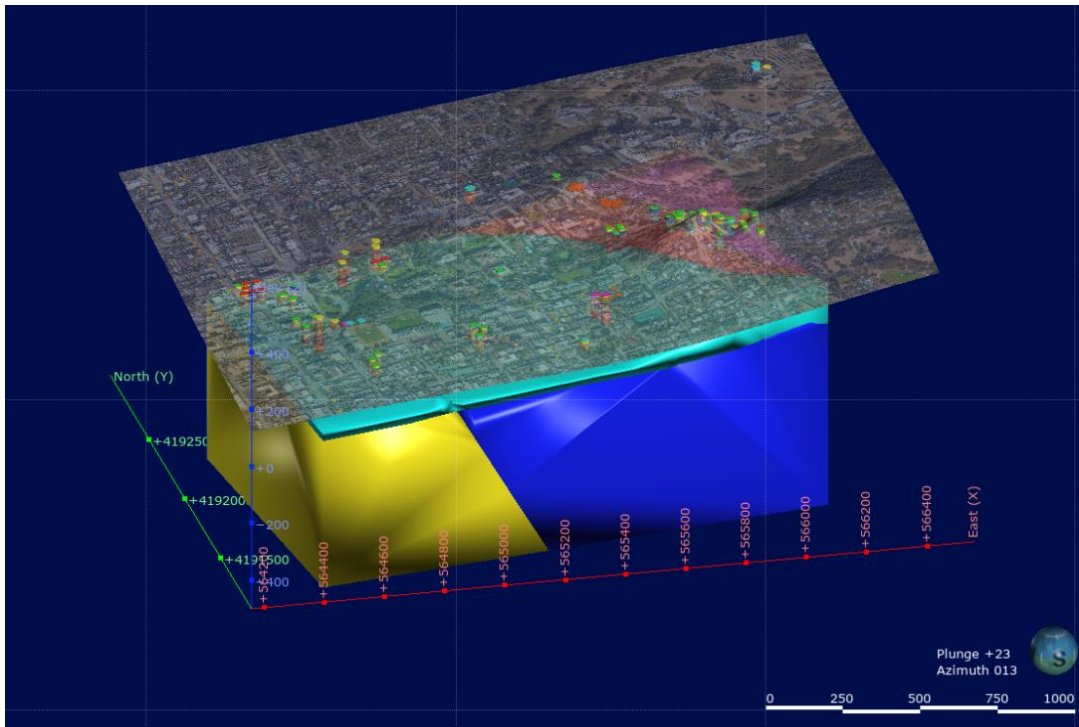


Figure 2.4 3-D geological model of Berkeley Campus

### 2.3.1 Alluvial Deposit

The surficial deposits of the Berkeley campus are roughly 40 ft of stiff to very stiff silty and sandy clay, overlying approximately 5 ft of hard clay and dense sand. The deposits are shown as the cyan region in Figure 2.4. These materials are alluvial deposits from the stream running down from Berkeley Hills, and they can be divided into older alluvial and younger alluvial. The older alluvial belongs to the Temescal formation of the late Pleistocene, mainly containing slightly consolidated clayey gravel and silty clay. The younger alluvials are deposits of the Holocene age. According to the boring logs and the 3D model, the deposits in the western and southern areas of the campus are relatively thicker (roughly 35 ft to 45 ft).

In comparison, the deposits in the central and northern regions of the campus are thinner (roughly 10 ft to 20 ft). In this research, a boring investigation was conducted near the University House (north of campus). The record indicates a 10-feet-deep clay layer overlying a 20-feet-deep clayey sandy gravel layer. The soil profile beneath the Berkeley campus can be summarized as follows:

- **Fill:** loose soil with grass and sawdust, 0 to 3 ft thick.
- **Upper Clay Layer:** stiff to very stiff clay, 20 to 40 ft thick.
- **Clay sand with gravel:** medium-dense sand and clayey sand, 5 to 10 ft thick.

- **Bedrock:** Franciscan Complex/Great Valley Sequence, very thick.

### **2.3.2 Bedrock**

The Berkeley Campus is right on the boundary of the Franciscan Complex and the Great Valley Sequence. Most of the bedrock beneath the campus is the Franciscan formation, composed of Jurassic and Cretaceous marine sediments with mild metamorphism, shown as the blue region in Figure 2.4. According to the site investigation reports, the Franciscan Complex is primarily graywackes embedded with shales, schist, and serpentinite. The outcrops of the Franciscan formation can be observed at several sites of the Berkeley Campus, such as the corner of Gayley Road and Hearst Avenue and Observatory Hill. On the east side of the Hayward fault, the bedrock turns to the Great Valley Sequence from Mesozoic marine sediments, shown as the red region in Figure 2.4. The rocks in this formation are large shale deposited in the marine setting with thick bodies of sandstone and minor conglomerate. These two formations contact each other and are overlain by alluvial deposits.

The depth of the bedrock varies at different sites on the campus. In the southwestern campus area, the bedrock is deeper and encountered at a depth of 40 to 50 ft; in the central and northern areas of the campus, the bedrock is relatively shallower and located at a depth of 10 to 30 ft. During the borehole investigation conducted near the University House on the north of campus, the Franciscan formation was encountered at a depth of 30 ft. The cuttings from the bedrock are mainly greywacke with interbedded shale, serpentinite, and quartz.

### **2.3.3 Seismic Setting**

The primary active fault affecting the Berkeley campus is the northwest striking Hayward fault, which is part of the San Andreas fault system. It traverses Berkeley Hills and goes through the northeast of the campus (right beneath California Memorial Stadium). The fault brings the Great Valley Sequence (shown as the red region in Figure 2.4) on the east into contact with the Franciscan Complex (shown as the blue region in Figure 2.4). Alluvial deposits overlie both formations. Figure 2.5 shows the fault's alignment and the Aquist-Priolo earthquake fault hazard zone. The southwest side of the Hayward fault is slowly creeping toward the northwest against the northeast side. The relative slippage creates a sheared band and

threats the building above or near the fault. Besides the sheared band along the fault alignment, the bedrock under the campus is, to some extent, sheared, broken, and eroded. It contains some clay under the effect of tectonic movement, forming weak sheared zones. During the boring investigation near the University House, two sheared zones with low hardness were encountered at a depth of 75 ft and 280 ft. In 1868, the Hayward fault generated a large earthquake with an estimated magnitude of 6.8, causing surface rupture extending for tens of kilometers. The Hayward fault is estimated to have a probability of 32 % rupturing in an earthquake of moment magnitude (M) 6.7 or larger before 2045 (Field & Biasi et al., 2015). Besides the Hayward fault, the Berkeley campus can also be shaken by the activity of other faults, including the San Andreas fault, Mount Diablo Thrust, Calaveras, etc.

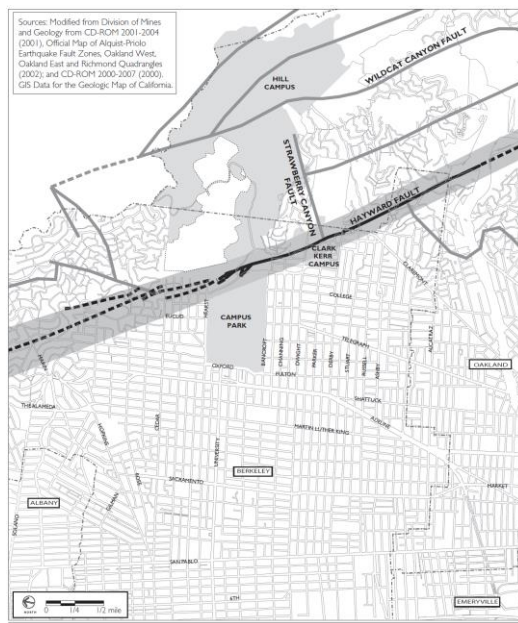


Figure 2.5 Fault system crossing the Berkeley Campus (Center, T., and Code, U. B.)

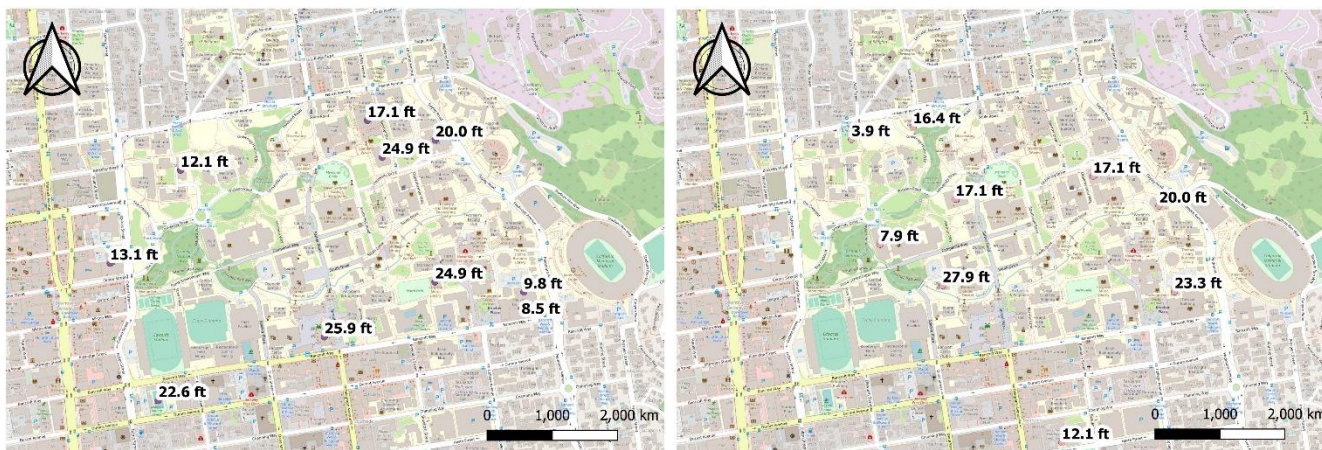
### 2.3.4 Liquefaction

Liquefaction refers to the loss of shear strength of saturated and cohesionless soil due to the build-up of excess pore pressure under seismic load. It usually happens in a sand layer below the water table. Although 5 ft to 10 ft thick of dense sand is likely to underlie the surficial clay at the campus site, there is a low risk of liquefaction because sands distributed beneath the campus are medium dense sands, clayey sands, and clayey sandy gravel. The excess pore pressure built-up during an earthquake in these dense sands is far from the requirement of liquefaction.

### 2.3.5 Groundwater

The groundwater under the Berkeley campus generally slopes downward to the south-southwest, flowing from Berkeley Hills to San Francisco Bay. It goes through geologic zones, including Berkeley Hills on the east side of the Hayward fault, the Hayward fault zone, and the alluvial plain beneath the campus. Due to the complex geological conditions, the groundwater table has a wide variation in different campus sites, ranging from 5 ft to 50 ft. On the northeast side of the Hayward fault, the groundwater is perched upon the interface between the unweathered rock bedrock and the overlying soil layer. On the southwest side of the Hayward fault, groundwater flows through the coarser alluvial materials at shallow depths toward the San Francisco Bay. Seasonal water table fluctuation is observed, probably caused by rainfall and temperature variation.

The water tables at different locations on the campus are extracted from previous in-situ boring investigation data. They are classified into different seasons and shown in Figure 2.6. Generally, the water table depth on the Berkeley campus ranges from 3.5 ft to 46 ft, corresponding to the geological background described earlier. On the northeast side of the Hayward fault, the water table is relatively deeper and more than 30 ft (e. g., California Memorial Stadium). The water table is relatively shallower on the southwest side of the Hayward fault, where the terrain is flatter. The water table depth ranges from 13 ft to 25 ft for the northeast campus and 18 ft to 38 ft for the southwestern campus. Although the water table data is not dense enough to perform seasonal variation analysis, significant differences in the water table between different seasons can still be observed. For the northwestern campus, the water table depth ranges from 4 ft to 17 ft in the spring after the rainy season and increases to roughly 30 ft in the fall after the dry season. For the southeastern campus, the water table depth is approximately 10 ft in spring, rising to around 7 m in summer and fall.



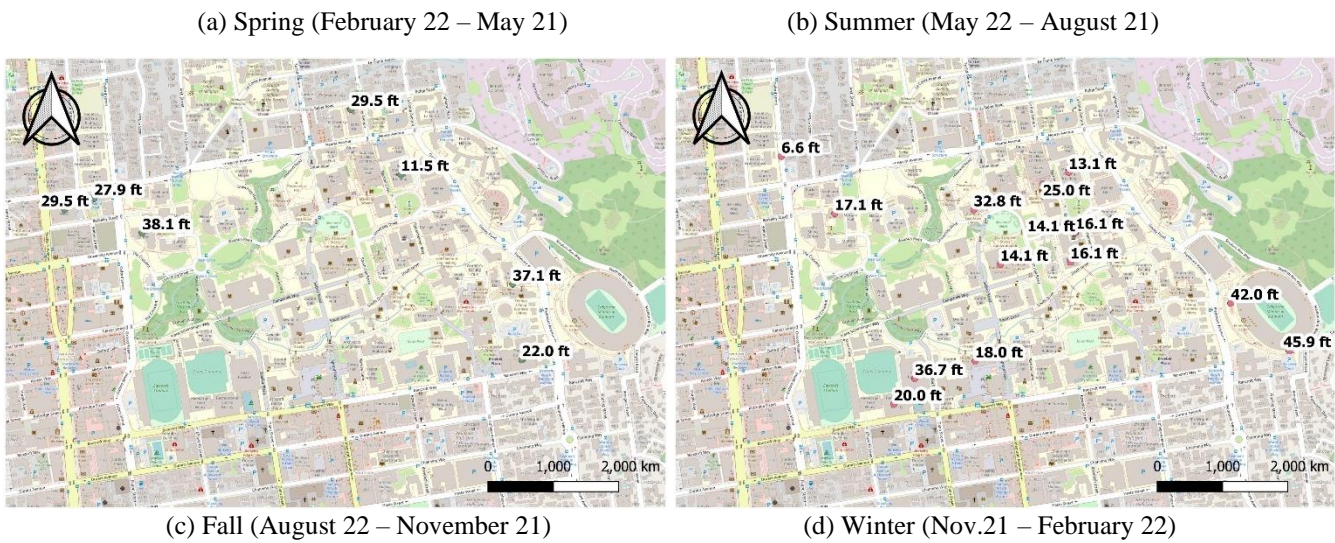


Figure 2.6 Distribution of water table in different seasons

### 3 Borehole Investigation

A borehole drilling and investigation was conducted on March 28 – April 1 near the University House located north of the Berkeley campus. The borehole is 400 ft deep with a diameter of 6 inches. The soil profile at the test site was logged during the drilling process, and geophysical logging was conducted after the drilling. This chapter summarizes the drilling process, the soil profile description, and the geophysical logging results.

#### 3.1 Drilling Process

The borehole location is shown in Figure 3.1. Since the borehole is roughly 400 ft deep and will encounter hard bedrock, the mud rotary drilling method was chosen. Soil/rock cores were not retrieved during the drilling process because the primary purpose of the borehole was to perform thermal response tests. However, the borehole was logged, and soil/rock cuttings returned by the mud were collected and stored in plastic bags every 5 ft during the drilling. The waste mud was then stored in a water tank and disposed of at a remote location for environmental consideration. The PITCHER company was hired to perform the drilling with Fraste FS-250 mobile drilling rig and MP-170-25C mud looping system, as shown in Figure 3.2. The equipment was transported to the site before the drilling started on March 25. The record of the drilling processes is described below, and the detailed drilling log is given in Appendix A.



Figure 3.1 Location of the borehole



Figure 3.2 Rotary drilling rig and mud loop system

**Day 1: Monday, March 28, light rain turns cloudy, 50 – 65 °F**

The drilling started at 7:23 am. An 8-ft-deep hole with a diameter of 8" was drilled, then an 8" tube and a box were installed for the mud loop. An 8" rotating bit was initially used, and the drilling speed was rapid when crossing the clay layer. At a depth of 30 ft, the bedrock (sandstone/greywacke) was encountered, and the bit was replaced by a 6" drilling bit. The drilling speed was relatively slow due to the hardness of the sandstone and accelerated a bit through the rock layer with more shale. Samples were grabbed every 5 ft and stored in plastic bags. The drilling stopped at 3:40 pm, and the borehole reached a depth of 125 ft on this day.

**Day 2: Tuesday, March 29, cloudy turn sunny, 53 – 65 °F**

The drilling was delayed due to refueling water and gas. It finally started at 9: 45 am. Samples were grabbed every 5 ft. The drilling stopped at 3:58 pm, and the borehole reached a depth of 255 ft.

**Day 3: Wednesday, March 30, sunny, 53 – 65 °F**

The drilling started at 7:12 am. Samples were grabbed every 5 ft. At a depth of 280 ft, a highly fractured sheared zone was encountered. The drilling speed became more rapid than usual, and some clay formed by eroded rock could be found in the returns. The drilling stopped at 3:58 pm, and the borehole reached a depth of 360 ft.

#### ***Day 4: Thursday, March 31, cloudy, 53 – 63 °F***

The drilling started at 7:20 am and reached 400 ft at 10:38 am. The rods and drilling bit were then pulled up, and the Norcal Geophysical Consultant logged the borehole. A caliper survey was first conducted to assess the stability of the borehole, and PS-wave velocities were then measured by PS-wave suspension logging. A televIEWER survey was also performed to map the interpretable discontinuities in the rock portion of the borehole. Finally, stratigraphic changes were investigated through natural gamma logging. The geophysical logging was finished at 8:30 pm.

#### ***Day 5: Friday, April 1, sunny, 55 – 67 °F***

At 7:00 am, a brief meeting was given to clarify the process of attaching the piezometer, geophone, and fiber optic sensors to the U-bend pipe. At 8:00 am, the installation of the pipe and sensors started. The sensors were first attached to the U-bend pipe using tape. The U-bend pipe was pushed down to the borehole using a 1" rod. Five fiber optic piezometers were installed at depths of 66 ft, 160.25 ft, 242 ft, 326 ft, and 397 ft, whereas four VW piezometers were installed at depths of 66 ft, 160.25 ft, 242 ft, 326 ft. One geophone was seated at a depth of 320 ft. The installation of the U-pipe and sensors was completed at 11:35 am, and grouting started at 2 pm. The grouting was interrupted by the jam of the tremie pipe at 2:50 pm when reaching a depth of 280 ft. Workers tried to dredge the pipe and restart the grouting at 5:00 pm but failed. The grouting was finally restarted at 8:00 pm and finished at 10:45 pm. To check the status of sensors and monitor the temperature change during the grouting process, the borehole temperature was measured using fiber optic sensors and temperature sensors from 3:00 pm to 12:00 pm.

### **3.2 Soil Profile Description**

According to the boring log recorded during the drilling process, the ground beneath the investigation site can be divided into four layers as follows:

- **Topsoil:** 0 – 1 ft, clay with some grass and sawdust.
- **Clay layer:** 1 – 10 ft, yellowish clay with some gravel, trace reddish chert can be found, orange mottling indicates oxidation due to water table fluctuation.
- **Gravel layer:** 10 – 30 ft, sandy gravel is underlying the clay layer. It is multicolor, well-graded sandy gravel, and trace clay can be found.

- **Franciscan Complex:** 30 – 400 ft, the bedrock underlying the gravel layer is the Franciscan Complex. At this specific site, it is the mélange of sandstone (greywacke), shale, and serpentinite. Sandstone is the primary material, and the content of interbedded shale varies according to depth. Trace serpentinite can also be found at some depths. Sheared zones were identified at depths of 75 ft, 200 ft, 280 ft, and 330 ft. The bedrock was sheared, fractured, and eroded under the tectonic effect, generating some clay that can be found in the cutting materials. The sheared zones are weaker and have lower mechanical properties than intact bedrock, so the drilling went faster when crossing these zones.

The detailed boring log is given in Appendix B.

### **3.3 Geophysical Logging**

The NORCAL Team was hired to conduct the borehole geophysical logging investigation. The main scope of work included: (i) a caliper survey for borehole stability analysis and diameter measure, (ii) a PS-wave Suspension survey to measure compression (P) and shear (S) wave velocity, (iii) a televiewer survey for discontinuity classification, and (iv) a natural gamma logging survey for stratigraphy mapping. The detailed investigation results are given in Appendix C, prepared by the NORCAL team.

#### **3.2.1 P-wave Velocity**

According to the P-wave logging, the water table is estimated to be 16 ft beneath the ground surface. The P-wave velocity in the upper 16 ft above the water table ranges between 2,800 ft/s and 3,350 ft/s. In the sediments between 18 to 23 ft depth, the P-wave velocity ranges from 6,000 ft/s to 8,410 ft/s. In the bedrock below 23 ft depth, the P-wave velocities recorded are between 9,000 ft/s to 18,700 ft/s.

#### **3.2.2 S-wave Velocity**

Results show that S-wave velocity varies among different types of stratigraphy. For the deposits above the depth of 24 ft, the S-wave velocity ranges between 870 ft/s and 2570 ft/s. For the bedrock below the depth of 24 ft, the S-wave velocity ranges between 3470 ft/s and 9380 ft/s. Lower S-wave velocity in the bedrock means high fracture density or significant weathering.

#### **3.2.3 Televiewer Logging**

Usually, for televiewer logging, a higher amplitude acoustic signal will be generated from a well-cemented zone. In comparison, a lower amplitude acoustic signal will be produced from weathered zones and

fractures. In this borehole, however, signal attenuation due to the thick drilling mud masked the variation of acoustic amplitude and gave a relatively consistent amplitude image.

The borehole deviation was also measured from the televIEWER logging. The average tilt from the vertical is less than 5 degrees above the depth of 230 ft, then increases to 10 degrees at a depth of 365 ft, and finally reaches 12 degrees at the bottom. Thus, the bottom of the borehole is approximately 12 ft west and 33 ft south of the borehole at the ground surface.

### **3.3.4 Natural Gamma Logging**

The natural gamma values from the borehole range between 25 and 125 APICs. The values higher than 120 APICs can be found at depths of 195 – 196 ft, 250 ft, 275 – 280 ft, and 325 – 327 ft. These high natural gamma values are probably the result of shale beds or weathered zones, which corresponds well with the record of borehole logging (see next).

## **3.4 Comparison of Geophysical Log and Boring Log**

Figure 3.3 compares the results of geophysical logging with the geological conditions recorded by the boring log. The changes in P-wave velocity ( $V_p$ ), S-wave velocity ( $V_s$ ), and natural gamma logging reflect well to the interface between the bedrock and sediment and the existence of weak shale layer and sheared zones. For example, for the deposits above 30 ft,  $V_s$ ,  $V_p$ , and natural gamma are roughly 1300 ft/s, 3000 ft/s, and 65 APICs, respectively. When encountering the sandstone (greywacke),  $V_s$ ,  $V_p$ , and natural gamma rise rapidly to 5500 ft/s, 13000 ft/s, and 80 APICs, respectively. At a depth of 75 ft, 200 ft, 280 ft, and 330 ft (marked as red lines in Figure 3.3), the existence of sheared zones or weak layers with higher content of shale causes a drop in the  $V_s$  and  $V_p$  profiles and a rise in the natural gamma profile. Since rotary drilling was used to drill the borehole and the borehole was logged based on the cuttings returned, the boring log may not be accurate enough and probably misses several sheared zones at a depth of 170 ft and 240 ft where  $V_p$  and  $V_s$  drops, and natural gamma rises (marked by blue lines in Figure 3.3). Generally, the geophysical investigation results match well with the boring log.

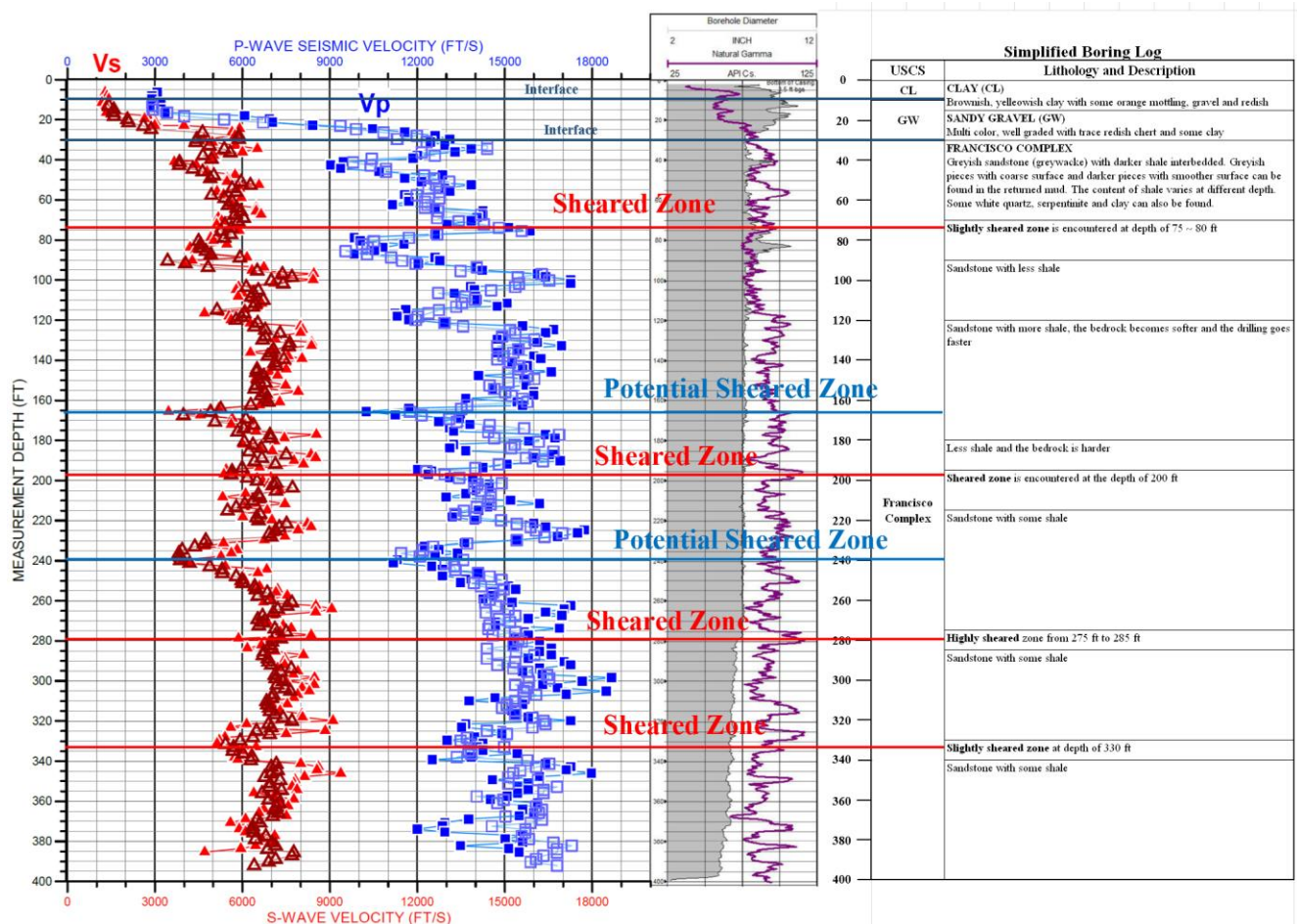


Figure 3.3 Comparison of Geophysical Log and Boring Log

## 4 Instrument Installation and Temperature Monitoring

The 400-ft monitoring borehole was drilled for measuring the geothermal properties and other research purposes. After the geophysical logging was finished, the geothermal heat looping pipe (U-pipe) with instruments attached was installed and grouted inside the borehole. To check the working status of instruments, temperature change along the borehole was recorded by distributed fiber optic sensors during grouting. This chapter gives the detailed instrument plan, describes the installation process, and analyzes the temperature change during grouting.

### 4.1 Instrument Plan

Sensors installed inside the borehole include Distributed Temperature Sensor (DTS), Strain Fiber Optic Sensor, FBG piezometer, Vibrating Wire Piezometer, and Short-Period Geophone. Figure 4.1 provides a brief configuration of the borehole, and detailed information about the devices is as follows:

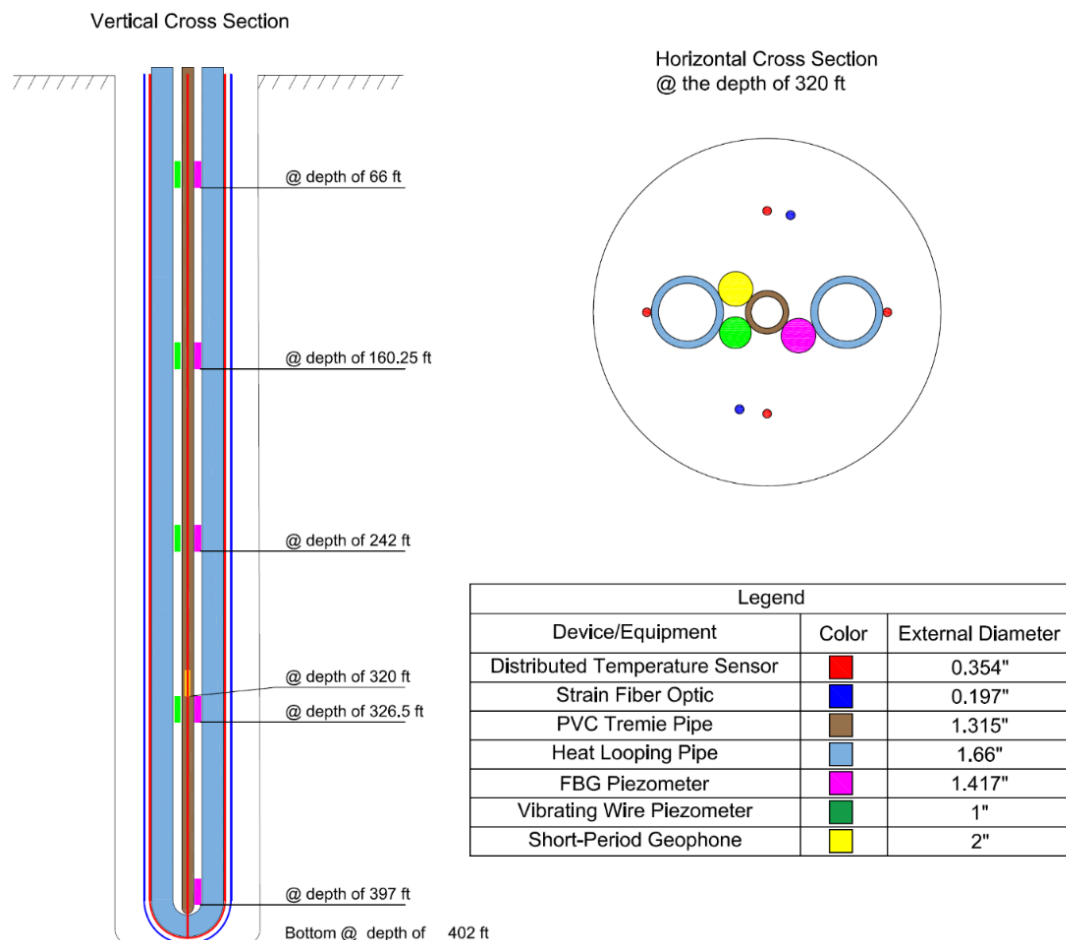


Figure 4.1 Configuration of the deep borehole

- **U-bend Looping Pipe** was produced and assembled by Centennial Plastic Inc. and installed by Pitcher Services, LLC. (<https://centennialplastics.com/products/geothermal/>). Two sections of 410-ft-long pipes (model number: 1.25" SDR 11) with an inner diameter of 1.25 inches were connected using an accommodated bullet U-bend fitting. They were produced in Centennial Plastic Inc.'s manufacturing facility and transported to the borehole site.
- **Distributed Fiber Optic Temperature Sensor (DFOS)** manufactured by BELDEN Inc. was used to measure the temperature ([https://catalog.belden.com/techdata/EN/FSSC004N0\\_techdata.pdf](https://catalog.belden.com/techdata/EN/FSSC004N0_techdata.pdf)). Outdoor Central Loose Tube OS2 4 Fibers (FSSC004N0) from BELDEN Inc. are designed for measuring temperature under harsh conditions. DTS was attached alongside the heat looping pipe and looped through the bottom of the borehole.
- **Strain Fiber Optic** from ETSC Technologies (NZS-DSS-C02) was used to measure strain change (<https://www.etsc-tech.be/upload/file/Strain%20sensing%20cable.pdf>). Two strain fiber optic cables were attached alongside the heat-looping pipe and looped through the bottom of the borehole.
- **FBG Piezometer** is a 100 kPa limit grouted piezometer with 0.05 kPa resolution and a 1536 – 1542 nm wavelength range (<https://citpo.com.tw/>). The length is 3.937 inches, whereas the diameter is 1.417 inches. For this borehole, five FBG piezometers were tied to the heat looping pipe at depths of 66 ft, 160.25 ft, 242 ft, 326.5 ft, and 397 ft, respectively.
- **Vibrating Wire Piezometers** were placed at the same depth as the FBG piezometer on the opposite side of the borehole. Four VW piezometers were installed at depths of 66 ft, 160.25 ft, 242 ft, and 326.5 ft, respectively.
- **Short-Period Geophone** was installed at a depth of 320 ft to record any ground motion. Three sensors vertically packaged inside the geophone record the motion in each direction. The geophone has a diameter of 2 inches and a height of 12 inches.

## 4.2 Instrument Installation

Distributed fiber optic cables and sensors were tied along the U-pipe using the tape, as shown in Figure 4.2. With the help of a rotatory drilling rig, an 1" hollow rod was used to push down the U-pipe with sensors attached gradually. During this process, the actual depths of the piezometers and geophones were

measured and recorded, which are shown in Figure 4.1. After installation, drillers gradually pumped in the grout through the hollow tremie pipe while pulling out the tremie pipe.



Figure 4.2 Installation of the heating pipe and instruments

## 4.3 Temperature Monitoring

### 4.3.1 Temperature Change during Grouting

The temperature variation along the borehole during grouting was measured using distributed fiber optic temperature sensor (DFOS). It should be noted that DFOS is attached to the U-pipe and tremie pipe, so below the grouting depth, DFOS measures the temperature of grouting ejected in the borehole. In contrast, above the grouting depth, DFOS measures the temperature of grouting inside the tremie pipe.

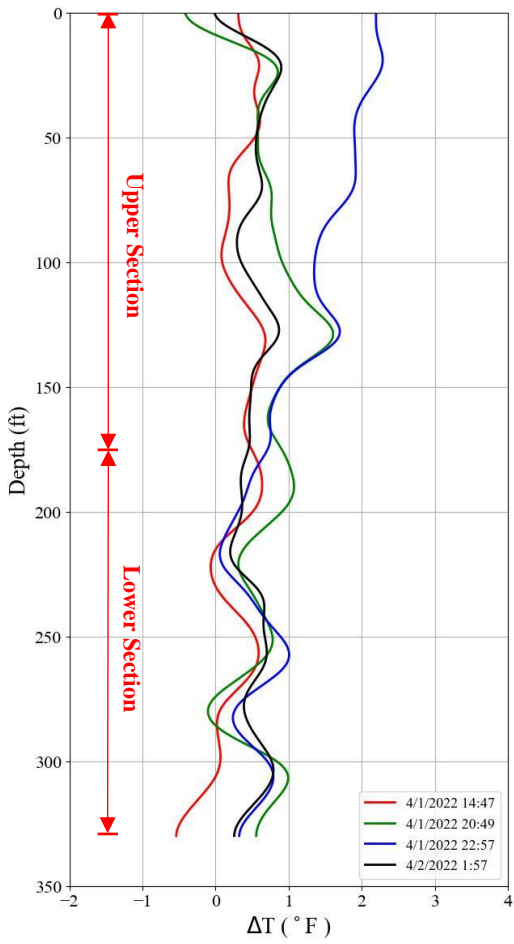
The frequency measured at 2:41 pm was chosen as the baseline to process the data. The grouting started at 2 pm; hence, the ground temperature used as the baseline is not the initial temperature but the disturbed ground temperature. The interruption of grouting at a depth of nearly 280 ft (recorded in the drilling log) may have affected the grouting quality and distributed fiber optic sensor. The sharp turn of the fiber optic cable at the bottom of the borehole also contributed to unreliable data. Thus, the data below the depth of 330 ft is removed from the plots.

The temperature rise recorded by DFOS is shown in Figure 4.3. As mentioned in the drilling process (section 3.1), the grouting started at 2 pm, was interrupted at 3 pm, restarted at 8 pm, and finished at 10:45 pm.  $\Delta T$  profiles shown in Figure 4.3 (a) indicate that at the end of grouting (blue line), temperature

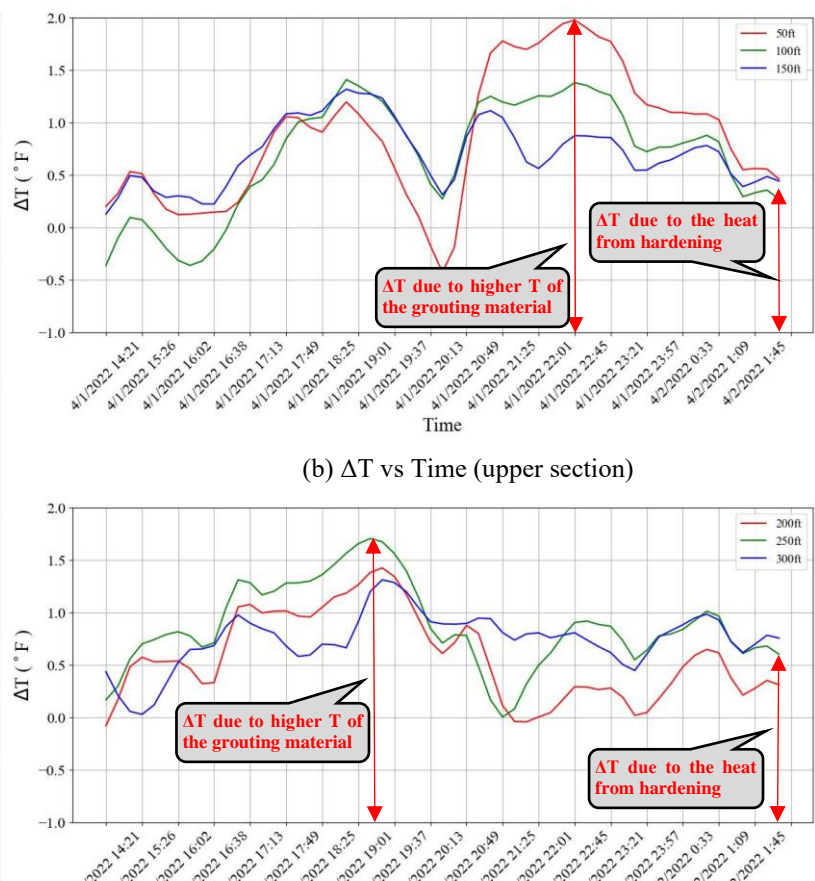
along the whole borehole increased by  $0.5 - 2$  °F. Since the elapsed time is not long enough for the hardening of the grouting material to release heat, the temperature rise is caused by the higher temperature of the grouting material. The temperature change decreases with depth because the deeper location has a higher initial ground temperature and is thus less affected by grouting. Three hours after the completion of grouting (black line), the temperature change decreases to roughly  $0.5$  °F. This slight temperature rise is caused by the heat released from the hardening of the grouting material.

Figure 4.3 (b) and (c) show curves of temperature change versus time at different depths, and temperature change pattern can also be reflected. The temperature change first reaches a peak value due to the higher temperature of the grouting material and decreases to a lower value. Due to the heat released from the hardening of the grouting material, the temperature is still  $0.5$  °F higher than the initial value. The lower section reached the highest temperature earlier than the upper section because the grouting of the bottom part was finished before the interruption of grouting at 2:50 pm. A significant temperature drop can be found in all curves of  $\Delta T$  versus time at roughly 8 pm. This is caused by measures drillers took to dredge the tremie pipe and restart the grouting.

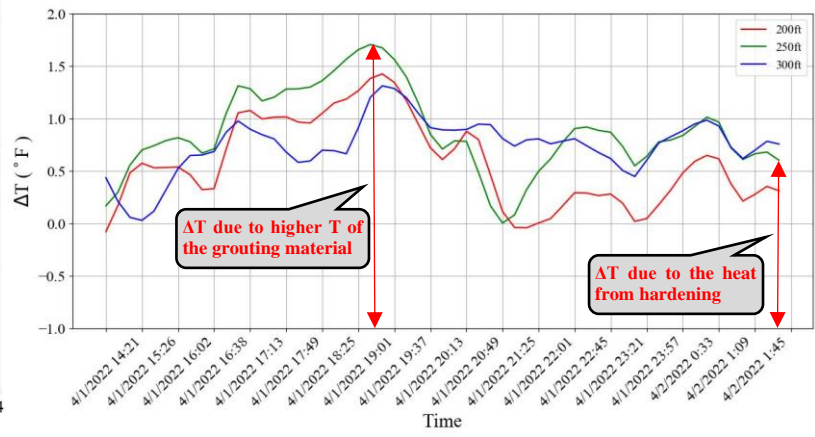
In conclusion, distributed fiber optic temperature sensors work well in recording the temperature variation during construction and revealing valuable patterns. Due to interruption and lack of data after 24 hours of grouting, it isn't easy to assess the grouting quality at different depths through the heat released from the hardening of the grouting material.



(a)  $\Delta T$  vs Depth



(b)  $\Delta T$  vs Time (upper section)



(c)  $\Delta T$  vs Time (lower section)

Figure 4.3 Change of temperature During the Grouting Process

#### 4.3.2 Geothermal Gradient

After the grouting of the borehole, ground temperatures at different depths were recorded using the VW piezometers at a one-month interval. Figure 4.4 shows the ground temperature profiles measured on different dates. Disturbed by the heat released from the hydration of grouting, the ground temperatures on April 4, immediately after grout placement, are  $0.5 - 1$  °F higher than the other dates. The sections at shallow depths are more affected by hydration. By excluding the disturbed ground temperature on April 4, the geothermal gradient is then calculated using the average ground temperature from April 22 to June 2. The measured geothermal gradient is  $0.0136$  °F/ft ( $24.79$  °C/km), which is similar to the normal range of the geothermal gradient ( $0.0137 - 0.0165$  °F/ft or  $25 - 30$  °C/km).

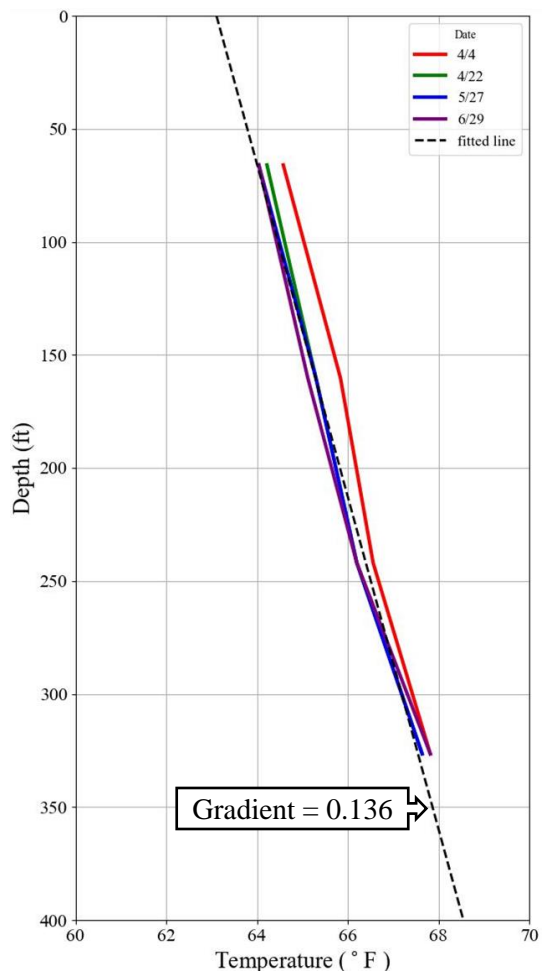


Figure 4.4 The Ground Temperature Profiles

## 5 Distributed Thermal Response Test

Distributed temperature sensors have been used in thermal response tests, known as distributed thermal response tests (DTRTs). From the spatiotemporal data, the spatial profile of geothermal properties in the subsurface can be determined, which helps us better estimate the geothermal potential and design the GSHP system. In this project, two DTRTs were conducted, and Distributed Fiber Optic Sensors (DFOS) were used to monitor the temperature during the thermal response test. This chapter introduces the installation of DFOS, TRT standards, and detailed test plans. The results of two TRTs are analyzed, and spatial profiles of thermal properties are calculated.

### 5.1 Installation of DFOS

A loop of DFOS was first attached outside the looping pipe and grouted in the borehole. To measure the temperature rise of the water fluid inside the pipe, two loops of DFOS were also installed inside the supply and return, respectively. These DFOS will also compare the performances of different sensor locations (inside or outside the looping pipe). Figure 5.1.1 provides the borehole configuration with detailed locations of DFOS.

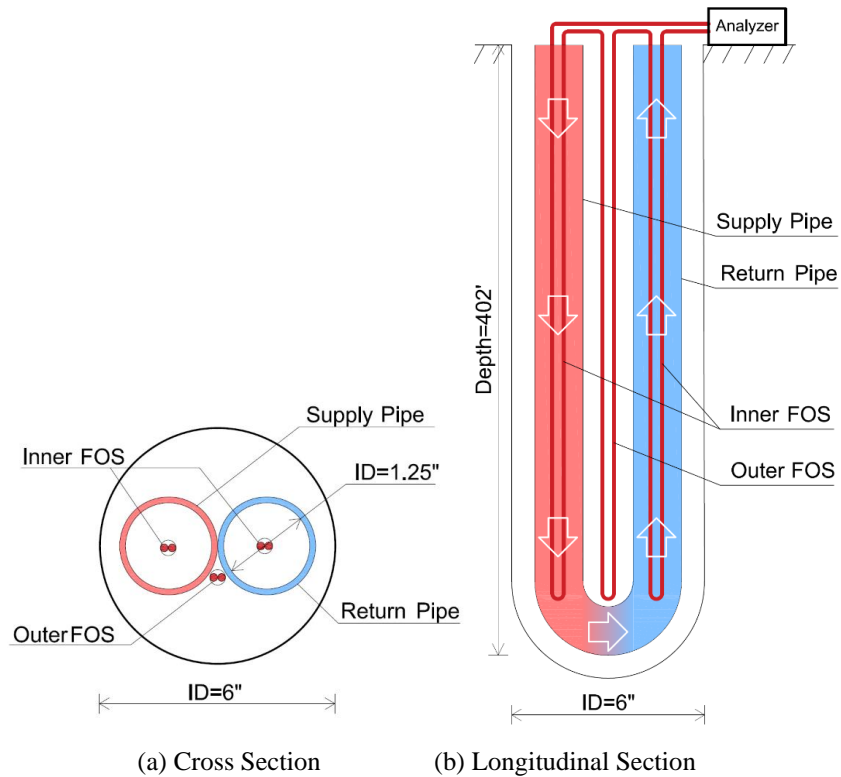


Fig. 5.1.1 Borehole Configuration

## 5.2 Thermal Response Test Plan

### 5.2.1 Test Standards

The American Society of Heating, Refrigeration, and Air Connection Engineers (ASHRAE) and the International Ground Source Heat Pump Association (IGSHPA) publish their recommended TRT standards. The key requirements from the 2014 ASHRAE handbook and the 2017 IGSHPA design and installation standards are given as follows:

- **The duration of the test** should be 36 to 48 hours. In this test, the duration was 48 hours for conservation.
- **The heat rate** should be 15 to 25 W/ft along the borehole, which means to achieve a heat rate of 20 W/ft for the 400-ft borehole, the required heating power of the TCT rig is roughly 8000 Watts.
- **The input power quality** should be stable, with a standard deviation of less than 1.5 % of the average value and peaks of less than 10 % of the average value.
- **Data collection frequency** should be at least every 10 min. The accuracy of the measured temperature should be within  $\pm 0.5$  °F, and the combined accuracy of the power transducer and recording device should be  $\pm 2$  % of the reading
- All piping above the ground should be covered using **heat insulation** material with a minimum thickness of 0.5 inches (e.g., foam insulation). The TRT rig should be enclosed in a sealed cabinet with a minimum of 1-inch insulation.
- **Flow rate** should be sufficient to provide a differential loop temperature of 6 to 12 °F.
- If retesting a bore is necessary, the loop temperature should return to the  $\pm 0.5$  °F pretest initial ground temperature.

### 5.2.2 Specific Procedures

The test equipment included a GRTI TRT rig, 20 kW diesel generator (Hertz Rental), fiber optic sensor, DFOS analyzer (OMNISENS/ALCIA), fish tape, water tank, two sections of pipe with an inner diameter of 4.25 inches, four pipe connection joints, heat insulation material, and self-fusion tape.

- **Step 1:** Install FOS inside the loop piping using Fish Tape.
- **Step 2:** Fill the looping pipe with water and wait for at least 10 hours until the water is in thermal equilibrium with the surrounding ground temperature.

- **Step 3:** Measure the undisturbed ground temperature through the VW piezometer and DFOS.
- **Step 4:** Connect the looping pipe to the TRT rig and cover the piping above the ground using heat-insulated material.
- **Step 5:** Turn on the pump of the TCT rig and loop the water for 1 hour without heating to get the formation temperature.
- **Step 6:** Turn on the heating element of the TCT rig with a total power of 8000 kW. The test will last for 48 hours.
- **Step 7:** While the test is run, record DFOS data through the analyzer every 2 mins.
- **Step 8:** Turn off the heating element and water pump and record the temperature decay for 12 – 24 hours.

## 5.3 First TRT Using OMNISENS (BOTDA)

The first TRT was performed between September 2 and 4, 2022, with the first heating phase of 46.6 hours and the second temperature decay phase of 12 hours. During the test, current, voltage, flow rate, and temperature change ( $\Delta T$ ) at the ground surface were recorded by GRTI TRT Rig. Brillouin Optical Time Domain Analyzer, OMNISENS, recorded the temperature change  $\Delta T$  along the borehole depth.

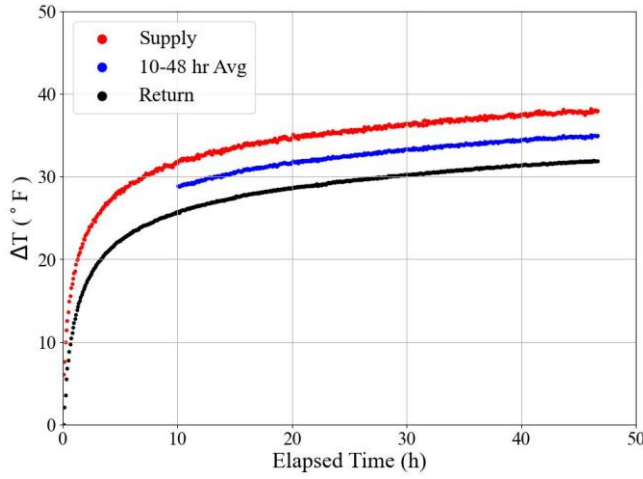
### 5.3.1 GRTI TRT Rig Data

The test statistics recorded by GRTI TRT Rig are summarized in Table 5.3.1. The heat input rate density and power quality well satisfy the TRT standards. The data of temperature change ( $\Delta T$ ) versus elapsed time in the supply and return pipes are shown in Figure 5.3.1. The "line source" method extracts the thermal conductivity from the average temperature rise between the supply and return pipes. The weighted average of heat capacity is calculated based on the boring log and specific heat and density values listed by Kavanaugh and Rafferty. Both thermal conductivity and heat capacity are then used to calculate the thermal diffusivity for this ground formation. The TRT report provided by GRTI is given in Appendix D, and the key thermal properties are summarized as follows:

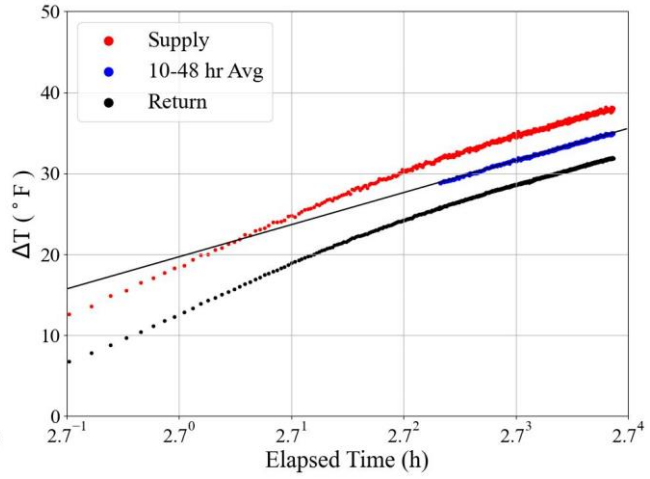
- Thermal conductivity: 1.38 Btu/hr-ft-°F.
- The weighted average of heat capacity: 36.8 Btu/ft<sup>3</sup>-°F
- Thermal diffusivity: 0.90 ft<sup>3</sup>/day

Table 5.3.1 Summary Test Statistics

Undistributed Formation Temperature	63.7 – 67.8 °F
Duration	46.6 hours
Average Voltage	241.5 V
Average Heat Input Rate	27936 Btu/hr (8185 W)
Average Heat Input Rate Density	69.5 Btu/hr-ft (20.4 W/ft)
Circulator Flow Rate	9.0 gpm
Standard Deviation of Power	0.62%
Maximum Variation in Power	2.39%



(a) Time in Normal Scale



(b) Time in Natural Log Scale

Fig. 5.3.1  $\Delta T$  vs. Elapsed Time at the Ground Surface

### 5.3.2 Inner DFOS Data

The inner DFOS recorded  $\Delta T$  of the fluid inside the pipe. OMNISENS was used to record the data every 2 mins with a spatial resolution of 0.837 ft (0.255 m) along the depth. Both  $\Delta T$  in the heating phase and temperature decay phase was recorded. Figure 5.3.2 shows the 2D contours of  $\Delta T$  versus depth and time. Subplots (a) and (b) show the raw  $\Delta T$  data recorded by the analyzer. To reduce the noise and analyze the spatial-temporal characteristics, the raw  $\Delta T$  data were smoothed using a 2D anisotropic Gaussian Filter with  $\sigma_{\text{time}}$  of 3 and  $\sigma_{\text{depth}}$  of 9. The filtered data are shown in subplots (c) and (d).

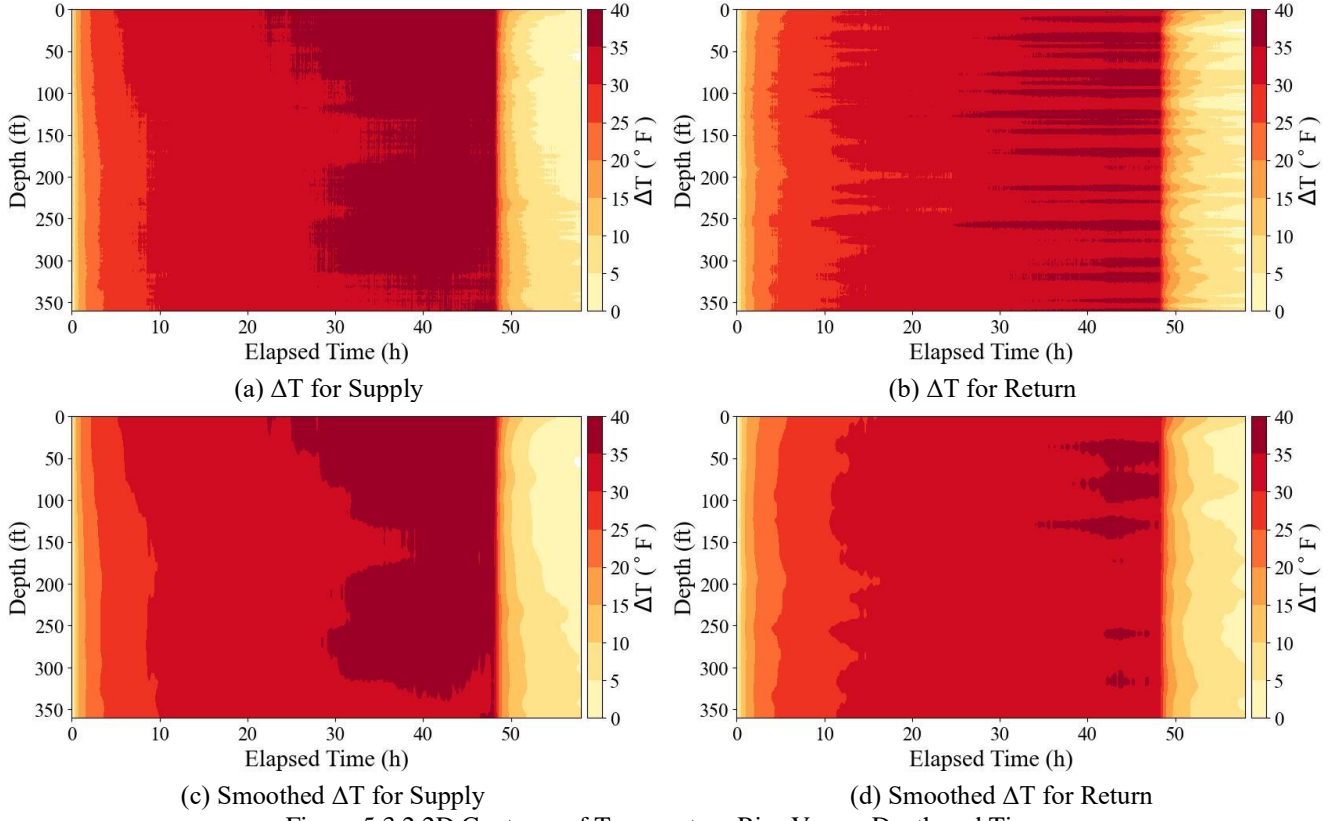


Figure 5.3.2 2D Contours of Temperature Rise Versus Depth and Time

To further analyze the data,  $\Delta T$  versus elapsed time at depths of 50 ft, 150 ft, 250 ft, and 350 ft are shown in Figure 5.3.3, respectively. Generally, the inner DFOS works well on capturing the patterns of  $\Delta T$  versus time at any depth during TRT. The final  $\Delta T$  is roughly between 34 – 37 °F, and  $\Delta T$  in the supply pipe is usually higher than  $\Delta T$  in the return pipe. The difference between  $\Delta T$  of the supply and return pipes is 2 – 3 °F, decreasing with depth. There is a very slight temperature drop at roughly 24 hours, probably caused by the fluctuation of the input power of the analyzer.

Figure 5.3.4 compares  $\Delta T$  at the ground surface measured by TRT Rig and DFOS. In the supply pipe,  $\Delta T$  measured by DFOS and GRTI Rig well match each other, while in the return pipe,  $\Delta T$  measured by DFOS is 2 – 3 °F higher than that measured by TRT Rig. Since TRT Rig measures the return temperature above the ground surface, while DFOS measures the return temperature beneath the ground surface, it is reasonable that  $\Delta T$  in the return pipe measured by the DFOS is slightly higher. Also, the spatial fluctuation of data along the depth in the return pipe may contribute to the mismatch of  $\Delta T$  in the return pipe, which is discussed in the following section, where the spatial distribution of  $\Delta T$  is analyzed.

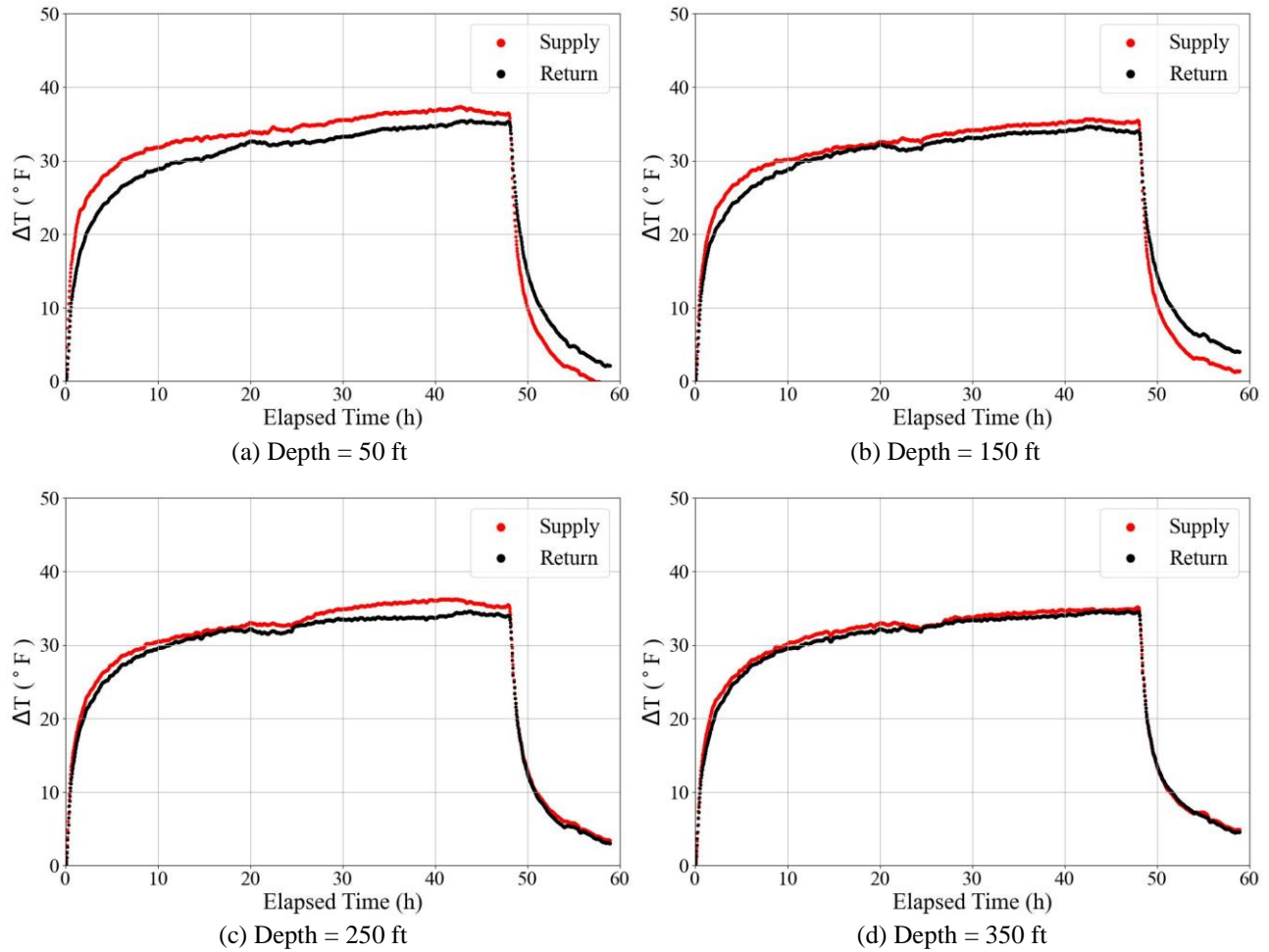


Fig. 5.3.3 T vs. Elapsed Time at Different Depths

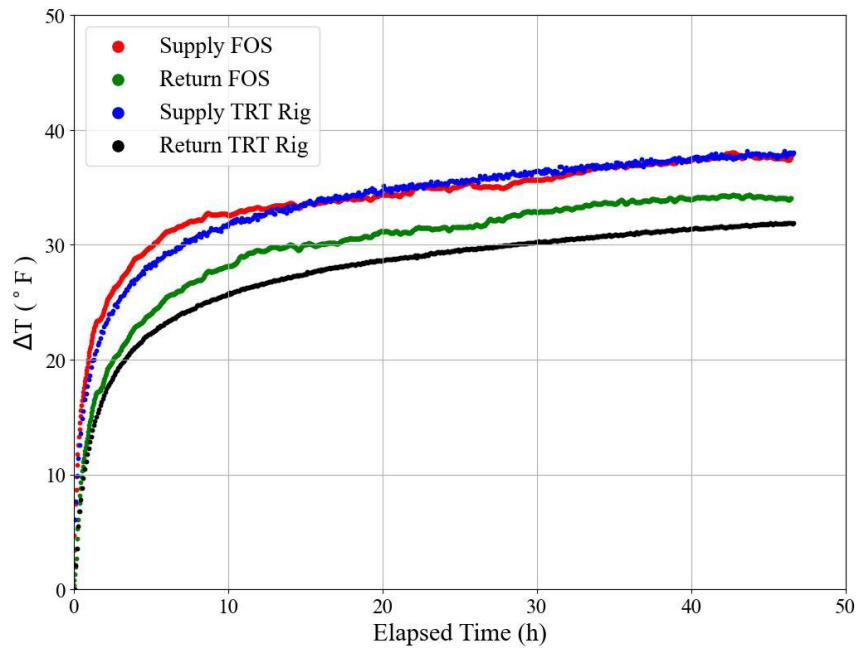


Fig. 5.3.4 Comparison of T vs. Elapsed Time at The Surface

Figure 5.3.5 divides the test data into the first 46.6-hour heating phase and the second 12-hour temperature decay phase, with elapsed time converted to a natural log scale. A linearity between  $\Delta T$  and natural log time can be observed in the two phases. The slopes are slightly different at different depths, indicating that thermal conductivity is variable in the subsurface. In the heating phase, the slight temperature drop seems to affect the calculation of the slopes. In the temperature decay phase, the 12-hour temperature monitor time might not be long enough to study the linearity because approximately 10 hours of reading is required to allow the early test error and the effect of finite borehole dimensions to become insignificant. This issue was fixed in the second TRT (see next) by extending the time to 24 hours.

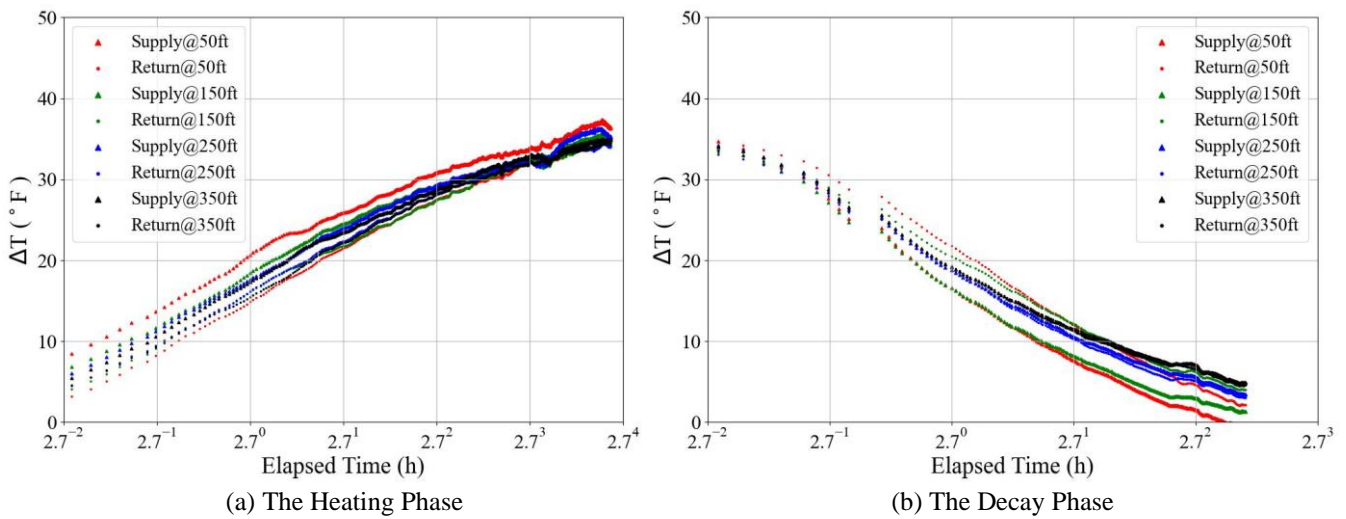


Fig. 5.3.5  $\Delta T$  vs. Elapsed Time in Natural Log Scale

Both raw and filtered  $\Delta T$  profiles at different times are shown in Figure 5.3.6. The  $\Delta T$  in the supply pipe decreases with depth, while  $\Delta T$  in the return pipe increases with depth, indicating a "V" shape. At the end of the heating phase, the temperature of the shallow surface increases by 34 – 38 °F, and the temperature near the bottom of the borehole increases by 35 °F. It is worth noting that the  $\Delta T$  values in the supply and return pipes converge at and below the depth of 250 ft, showing that the total temperature gradient of a certain depth below 250 ft is near zero. Heat transfer efficiency from the looping pipe to the ground at this depth is low. This may be related to sheared zones below 250 ft (250 ft, 275 – 280 ft, and 325 – 327 ft). Another possible reason is the poor grouting quality caused by the interruption of the grouting process at a depth of 280 ft (see Section 3.1). Fluctuation of  $\Delta T$  can be observed even in the smoothed profiles, especially in the return pipe. Several reasons can potentially contribute to this, among which the most important is the variation in grouting quality along the depth. Grouting quality can affect the heat transfer efficiency between the looping pipe and surrounding soil, thus leading to a variable

temperature profile. Geological characteristics such as sheared zones can also affect the temperature by changing the thermal conductivity of the layer.

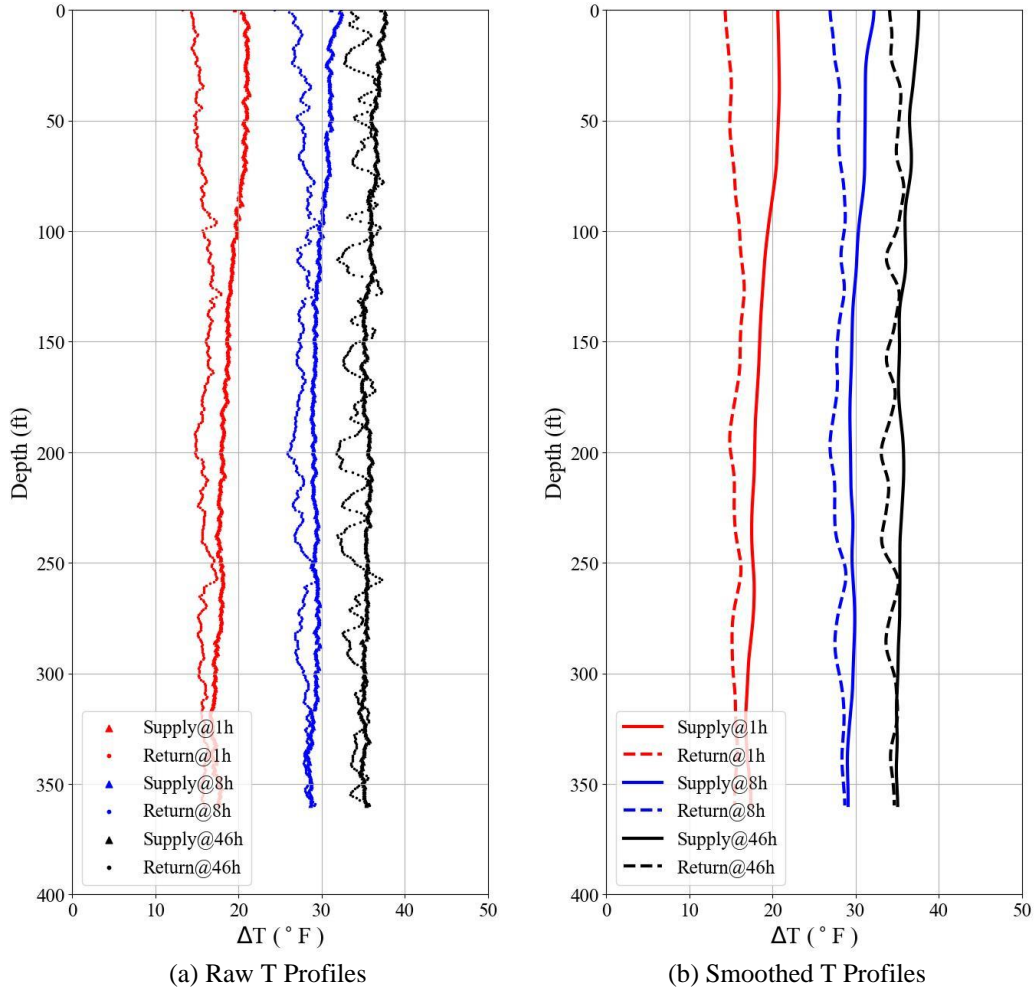


Figure 5.3.6 vs. Elapsed at Different Times

### 5.3.3 Outer DFOS Data

The  $\Delta T$  outside the looping pipe was recorded with a time interval of 2 mins and a spatial resolution of 0.837 ft (0.255 m). Figure 5.3.7 provides the 2D contours of raw and smoothed  $\Delta T$  versus depth and time.

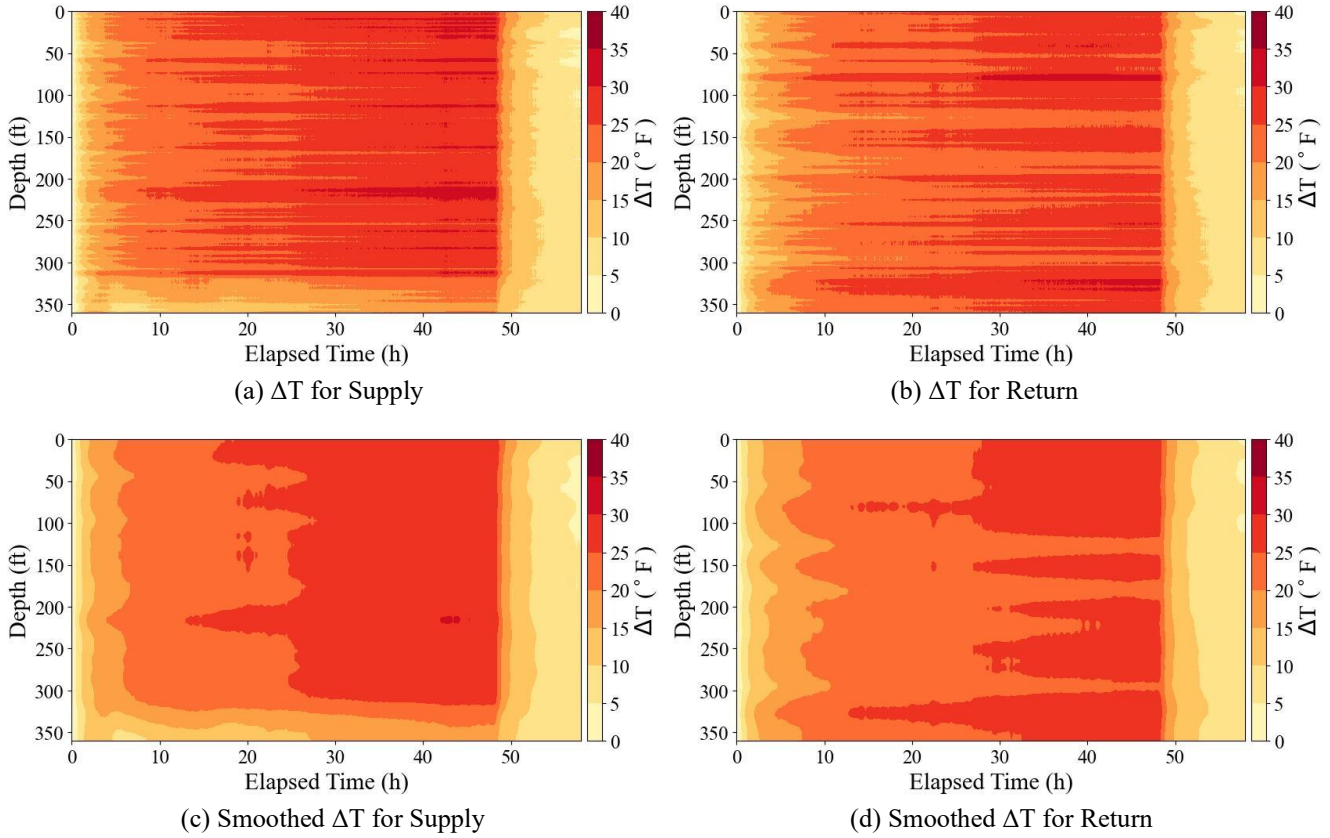


Figure 5.3.7 2D Contours of Temperature Rise Versus Depth and Time

$\Delta T$  versus elapsed time at depths of 50 ft, 150 ft, 250 ft, and 350 ft are shown in Figure 5.3.8. The final  $\Delta T$  outside the pipe is between 26 – 38 °F, which is nearly 9 °F lower than  $\Delta T$  inside the pipe. This is reasonable since the outer DFOS is embedded in the grout. There is no specific pattern of whether the supply or return pipe has a higher temperature rise. A slight temperature drop can be observed at roughly 24 hours at all depths, similar to the data inside the pipe. This is caused by the transient change of the power that supplies the DFOS analyzer. There is an anomaly in  $\Delta T$  of the supply pipe at a depth of 360 ft after 2 hours, as shown in Figure 5.3.8 (d). This is probably related to the anomaly in the grout at this depth and will be explained in the following section when the  $\Delta T$  profiles along the depth are discussed.

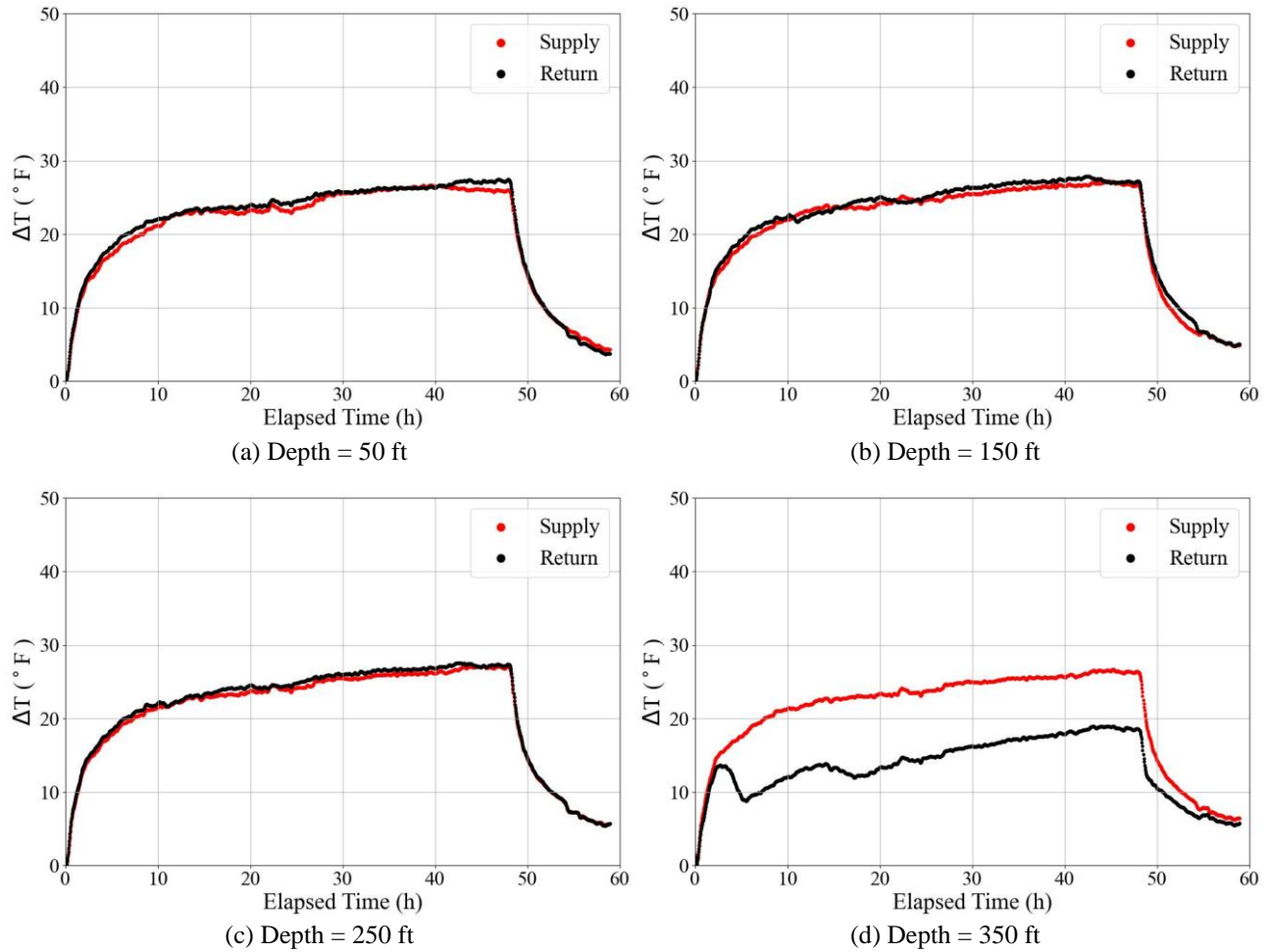


Fig. 5.3.8 T vs. Elapsed Time at Different Depths

As shown in Figure 5.3.9, the test data is divided into the first 46.6-hour heating phase and the second 12-hour decay phase, with elapsed time converted to a natural log scale. The pattern is similar to that of the inner DFOS data. A linearity between  $\Delta T$  and natural log time can also be observed in both phases, with slightly different slopes at different depths.

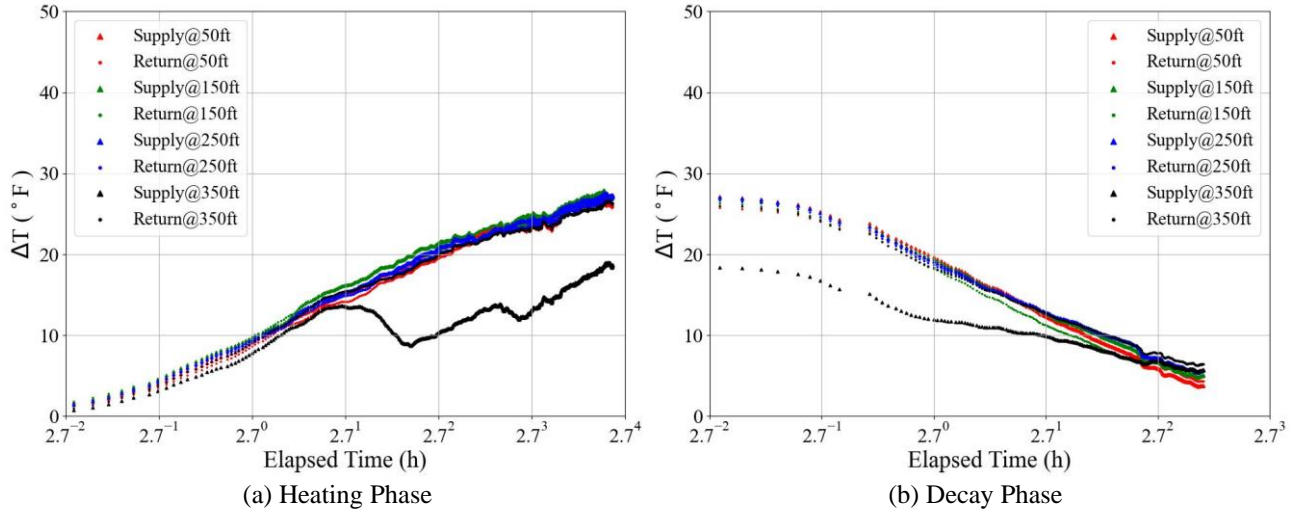


Fig. 5.3.9  $\Delta T$  vs. Elapsed Time in Natural Log Scale

Both raw and filtered  $\Delta T$  profiles at different times are shown in Figure 5.3.10. Unlike the  $\Delta T$  inside the pipe, the outer  $\Delta T$  profiles do not show the V-shape. Instead, the  $\Delta T$  of the supply and return pipes are very close to each other at the same depth. This is due to the position of the DFOS outside the pipe: DFOS are attached to the supply and return pipes (see Figure 5.1.1). Since they are not perfectly separated and attached to the target pipes but close to each other and twisting together, the  $\Delta T$  measured by them can be very close. At the end of the test, the temperature of the shallow surface increases by 27 – 30  $^{\circ}\text{F}$ , and the temperature near the bottom of the borehole increases by 27  $^{\circ}\text{F}$ , which is roughly 9  $^{\circ}\text{F}$  lower than the inner DFOS.

Similar to the inner  $\Delta T$ , the outer  $\Delta T$  in the supply and return pipes converge at and below the depth of 250 ft, meaning weak heat transfer from the looping pipe to the ground. Besides, the temperature rise data below the depth of 310 ft is abnormal, the same anomaly shown in Figure 5.3.8 (d). The observed weak heat transfer is likely related to the poor grouting below this depth. According to the drilling log (see Section 3.1), the grouting of the borehole was stopped due to jamming of the tremie pipe when reaching the depth of 280 ft and was restarted 5 hours later.

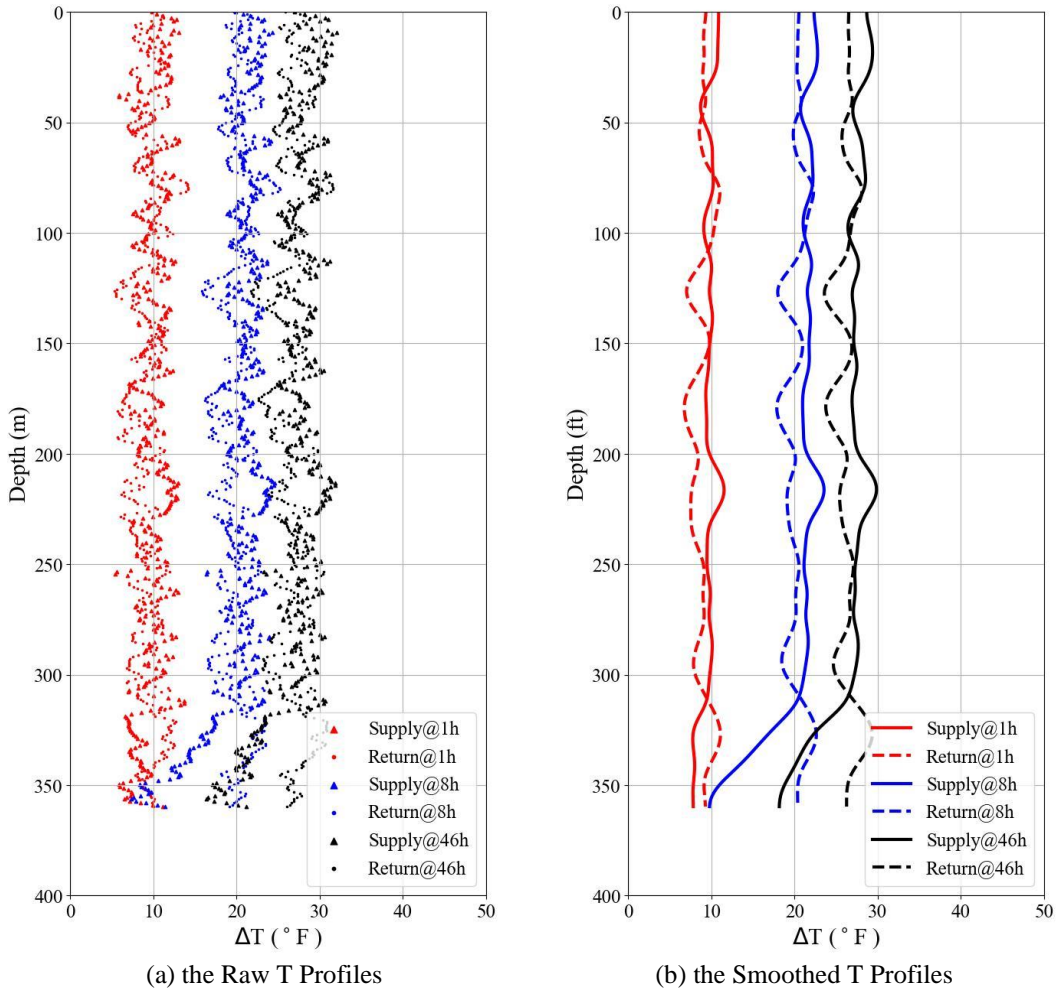


Figure 5.3.10 T vs. Elapsed at Different Times

## 5.4 Second TRT Using ALICIA (BOTDR)

The second TRT was performed between September 31 and October 2, 2022, with the first heating phase of 47.5 hours and the second temperature decay phase of 24 hours. During the test, current, voltage, flow rate, and temperature change at the ground surface are recorded by GRTI TRT Rig. Brillouin Optical Time Domain Reflectometer, ALICIA, recorded the temperature change ( $\Delta T$ ) along the depth.

### **5.4.1 GRTI Data**

The test statistics recorded by GRTI TRT Rig are summarized in Table 5.4.1. The heat input rate density and power quality well satisfy the TRT standards. The temperature change  $\Delta T$  versus elapsed time in the supply and return pipes are plotted in Figure 5.4.1. The TRT report supplied by GRIT is given in Appendix E, and the key thermal properties are summarized as follows:

- Thermal conductivity: 1.35 Btu/hr-ft-°F
- The weighted average of heat capacity: 36.8 Btu/ft<sup>3</sup>-°F
- Thermal diffusivity: 0.88 ft<sup>3</sup>/day

Table 5.4.1 Summary Test Statistics

Undistributed Formation Temperature	64.3 – 68.0 °F
Duration	47.5 hours
Average Voltage	238.7 V
Average Heat Input Rate Density	26,866 Btu/hr (7,872 W)
Average Heat Input Rate	66.8 Btu/hr-ft (19.6 W/ft)
Circulator Flow Rate	8.8 gpm
Standard Deviation of Power	0.50%
Maximum Variation in Power	1.94%

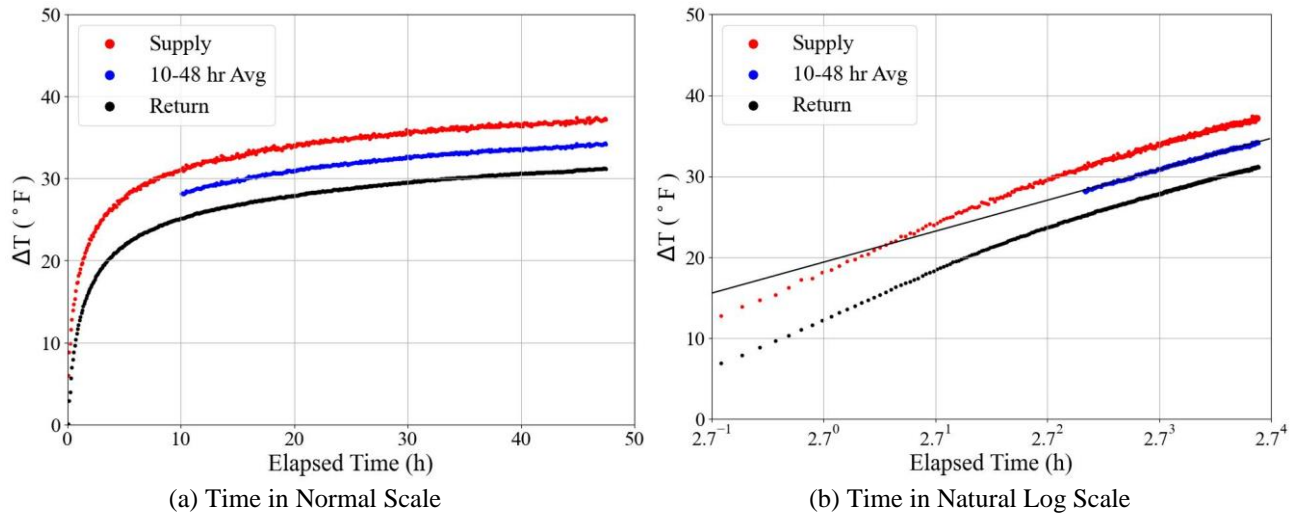


Fig. 5.4.1 T vs. Elapsed Time at the Ground Surface

### 5.4.2 Inner FOS Data

The inner DFOS recorded the  $\Delta T$  of fluid inside the pipe. The research team developed the ALICIA BOTDR analyzer to record the data every 2 mins with a spatial resolution of 0.328 ft (0.1 m). Both  $\Delta T$ s in the heating phase and temperature decay phase were recorded. Figure 5.4.2 provides the 2D contours of  $\Delta T$  versus depth and time. Subplots (a) and (b) show the raw  $\Delta T$  recorded by the analyzer. To reduce the noise and analyze the spatial-temporal characteristics,  $\Delta T$  was smoothed with data using a 2D anisotropic Gaussian Filter with  $\sigma_{\text{time}}$  of 3 and  $\sigma_{\text{depth}}$  of 20 (higher due to higher spatial resolution). The filtered data are presented in subplots (c) and (d).

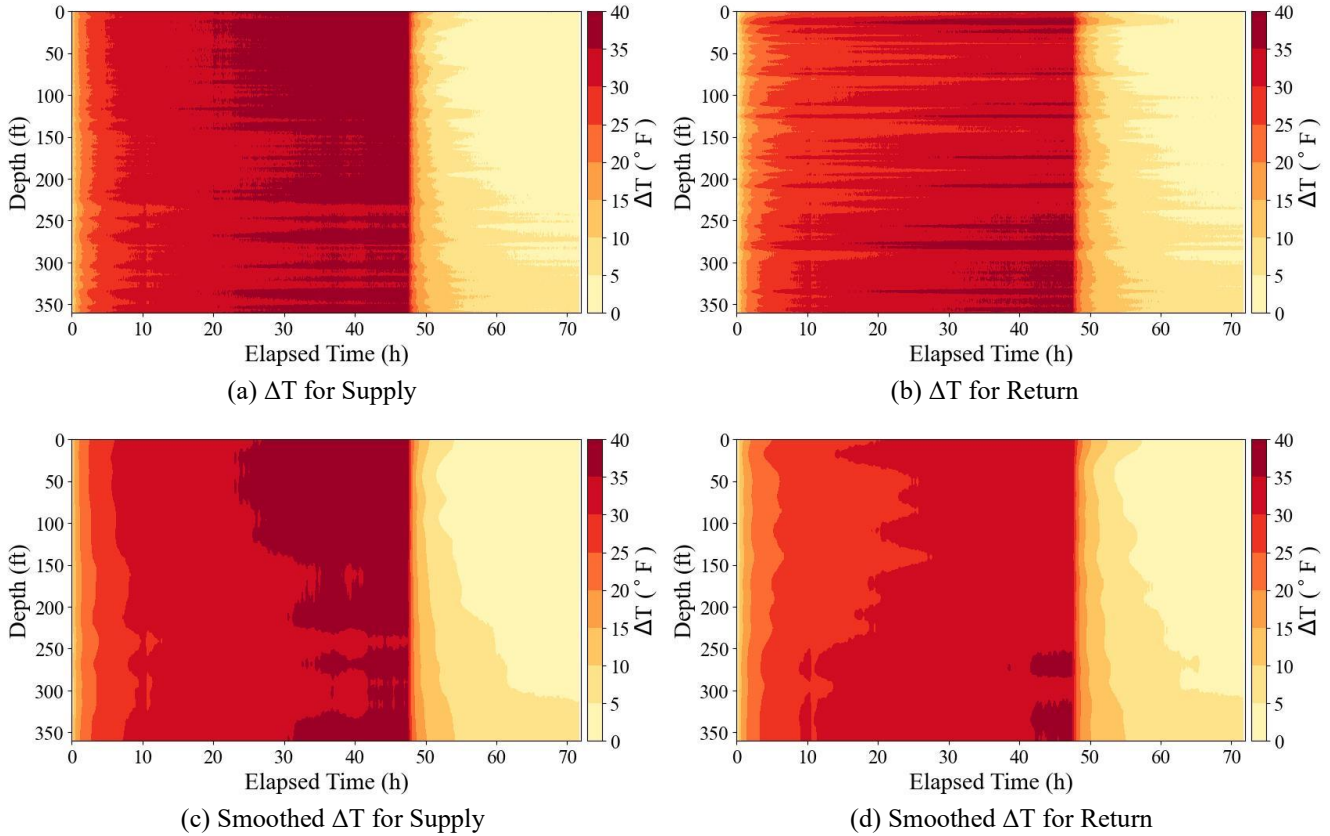


Figure 5.4.2 2D Contours of Temperature Rise Versus Depth and Time

To further analyze the data,  $\Delta T$  versus elapsed time at depths of 50 ft, 150 ft, 250 ft, and 350 ft are shown in Figure 5.4.3. The general patterns are almost the same as those of the first TRT. The temperature at the end of the heating phase increases by  $32 - 37$  °F, and  $\Delta T$  in the supply pipe is higher than  $\Delta T$  in the return pipe. The supply and return pipe temperature difference is roughly 5 °F, decreasing with depth and reaching zero at 250 ft. A systematic temperature offset of approximately 1 – 2 °F can be found at 11 hours, which is caused by a sudden decrease in the input voltage of ALICIA. However, this will not affect the TRT interpretation results because the data before roughly 10 hours have early test error and is affected by the finite borehole dimensions. Figure 5.4.4 compares  $\Delta T$  at the ground surface measured by the TRT Rig and DFOS, and the pattern is generally similar to that in the first test. In the supply pipe,  $\Delta T$  measured by DFOS and GRTI Rig well match each other, while in the return pipe,  $\Delta T$  measured by DFOS is 2 – 3 °F higher. The same reasons in section 5.3.2 can explain this and thus are not repeated.

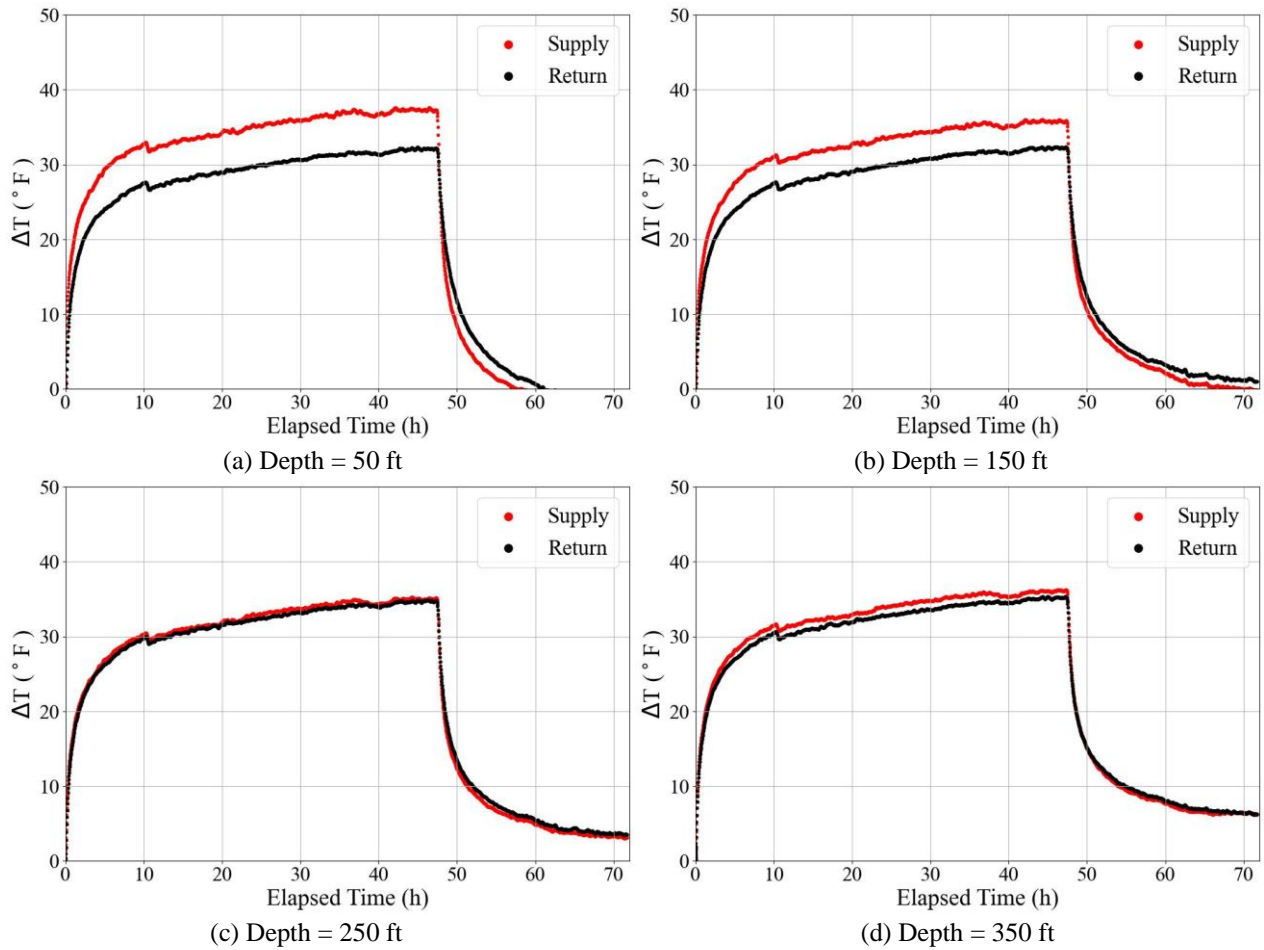


Fig. 5.4.3 T vs. Elapsed Time at Different Depths

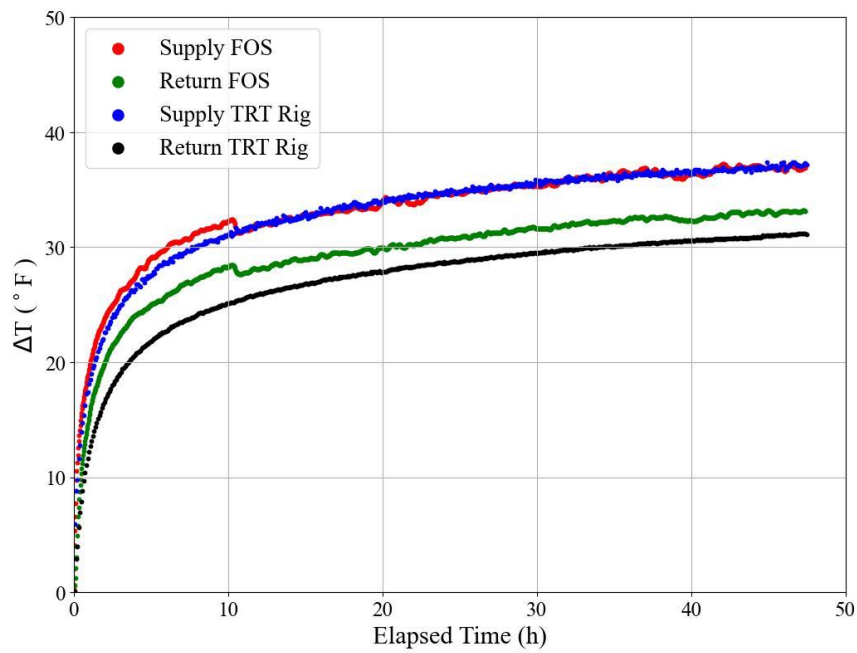


Fig. 5.4.4 Comparison of T vs. Elapsed Time at The Surface

Figure 5.4.5 shows the test data in the 48-hour heating phase and the 24-hour temperature decay phase, with elapsed time converted to a natural log scale. The linearity between  $\Delta T$  and natural log time is better than that of the first TRT. The offset of  $\Delta T$  does not affect the analysis of the slopes. It is worth noting that, at the end of the temperature decay phase, the curves of  $\Delta T$  versus natural log time do not seem linear and the scatter tends to be gentler. Since there's no direct heat input during the temperature decay phase, the pattern change is caused by the dissipation of residual heat into the ground.

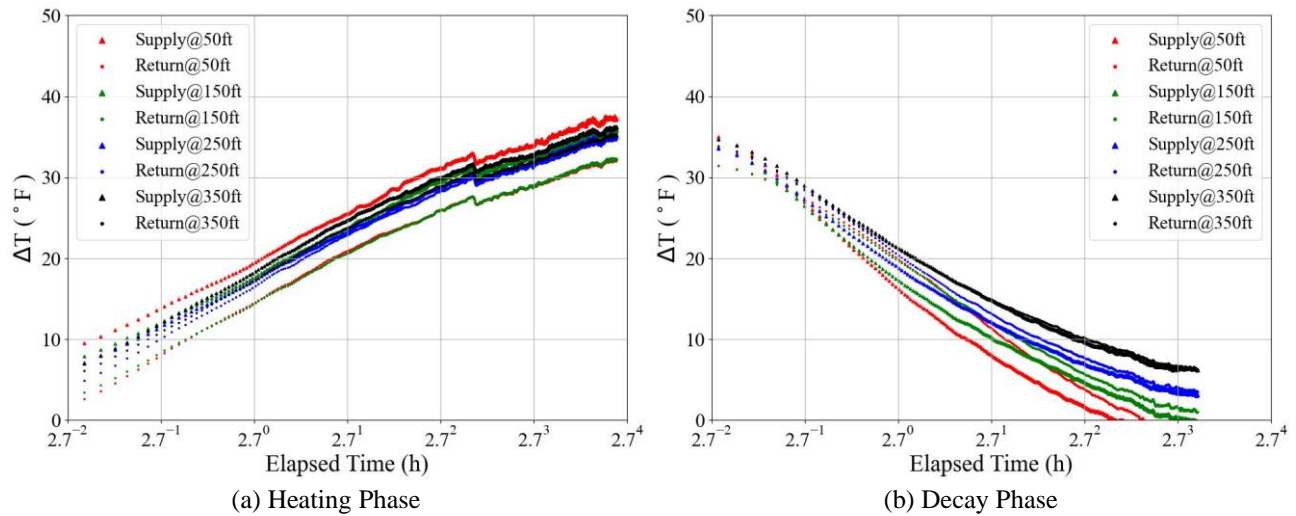


Fig. 5.4.5 T vs. Elapsed Time in Natural Log Scale

Both raw and filtered  $\Delta T$  profiles at different times are shown in Figure 5.4.6. The  $\Delta T$  in the supply pipe decreases with depth while  $\Delta T$  in the return pipe increases, forming a "V" shape. At the end of the test, the temperature of the shallow surface increases by  $30 - 37$  °F, and the temperature near the bottom of the borehole increases by roughly  $35$  °F. Same as the first TRT, the  $\Delta T$  in the supply and return pipes converge at a depth of 250 ft instead of the bottom, further verifying that there is weak heat transfer between the U-bend pipe and ground under the depth of 250 ft. Fluctuations of  $\Delta T$  caused by the variation in the geological conditions and grouting quality can be observed.

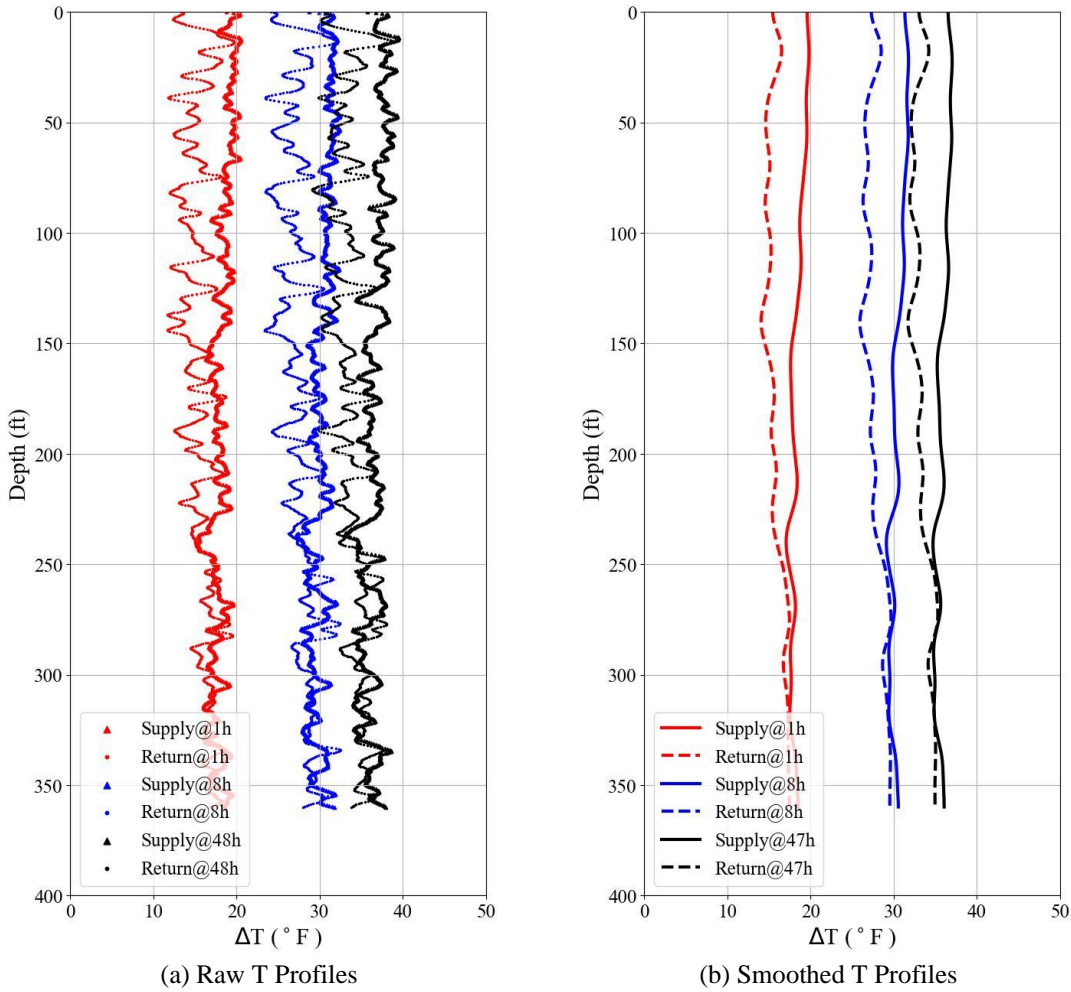
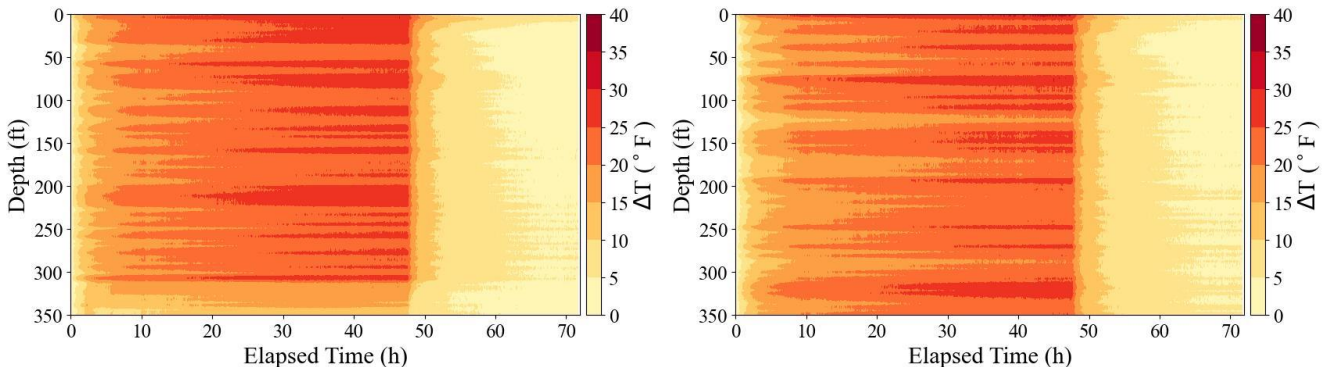


Figure 5.4.6 vs. Elapsed at Different Times

### 5.4.3 Outer DFOS Data

The temperature change outside the looping pipe was recorded with a time interval of 2 mins and a spatial resolution of 0.328 ft (0.1 m). Figure 5.4.7 shows the 2D contours of both raw and smoothed  $\Delta T$  versus depth and time.



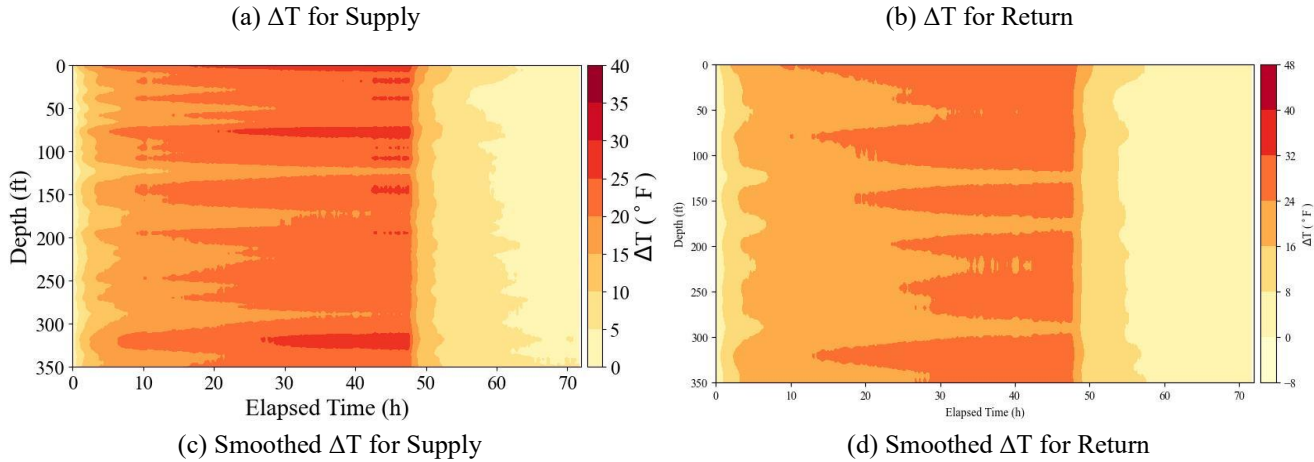
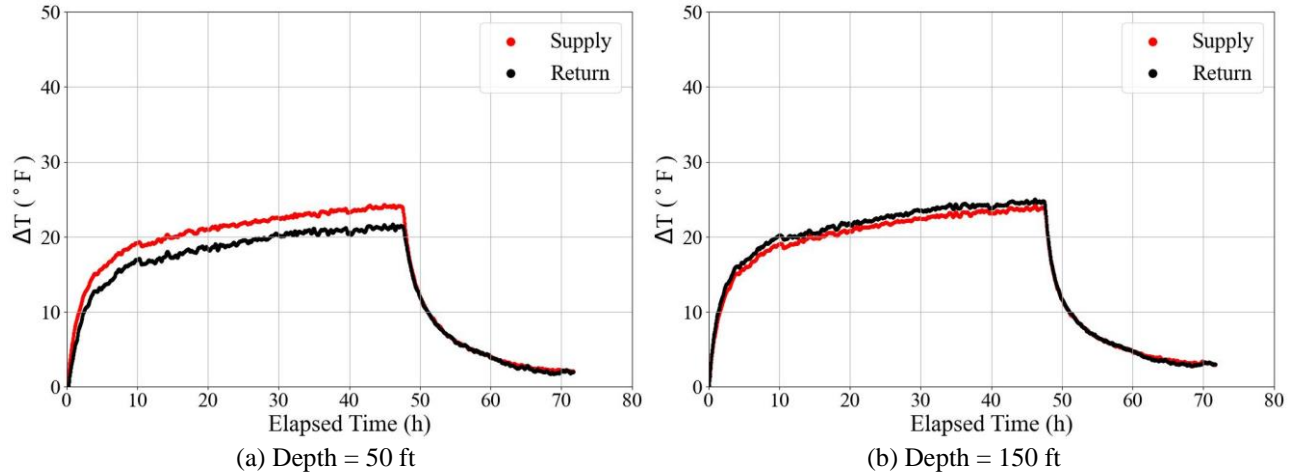


Figure 5.4.7 2D Contours of Temperature Rise Versus Depth and Time

Figure 5.4.8 shows the change of smoothed  $\Delta T$  versus elapsed time at depths of 50 ft, 150 ft, 250 ft, and 350 ft. The final  $\Delta T$  outside the pipe is roughly between 21 – 25 °F, which is nearly 9 °F lower than  $\Delta T$  inside the pipe. The  $\Delta T$  of the supply and return pipes are very close, which will also be observed in the following  $\Delta T$  profile figures. There is no specific trend in the relation of  $\Delta T$  of the supply and return pipes. An anomaly in  $\Delta T$  of the supply pipe at a depth of 360 ft can be observed in Figure 5.3.8 (d), and the possible reasons are given in Section 5.3.3.



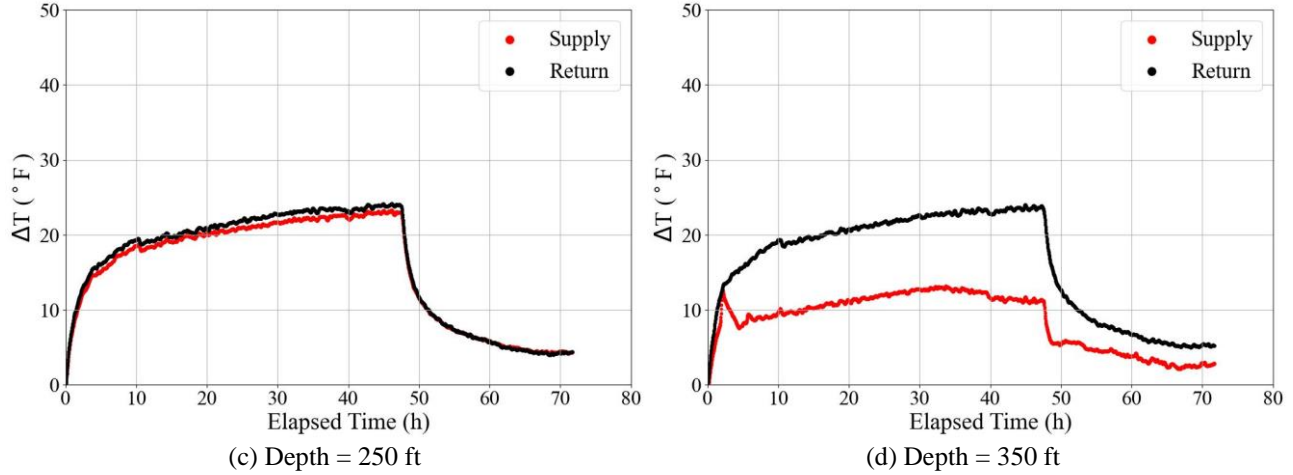


Fig. 5.4.8 T vs. Elapsed Time at Different Depths

Figure 5.4.9 shows the test data in the 48-hour heating and 24-hour temperature decay phases, with elapsed time converted to a natural log scale. A linearity between  $\Delta T$  and natural log time can be observed in both phases with slightly different slopes at different depths. Similar to the observations made in the first TRT,  $\Delta T$  versus natural log time at the end of the temperature decay phase tends to be flatter. As previously discussed, this is related to the dissipation of residual heat into the ground.

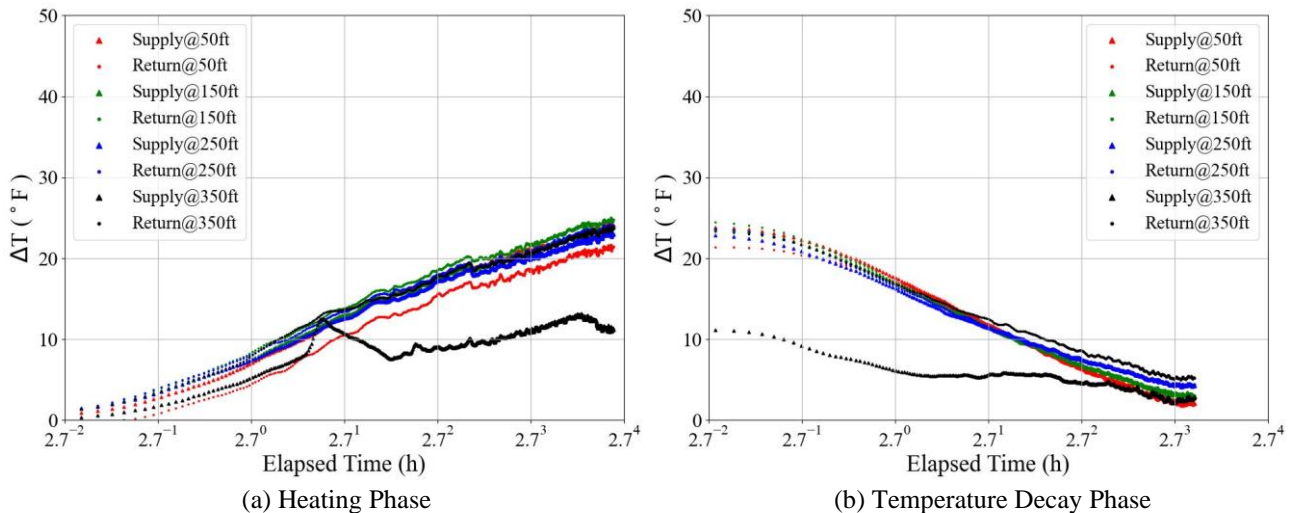


Fig. 5.4.9  $\Delta T$  vs. Elapsed Time in Natural Log Scale

Both raw and filtered  $\Delta T$  profiles at different times are shown in Figure 5.3.10. The  $\Delta T$  profiles in the supply and return pipes are very close because the DFOS for the supply and return pipes are installed close to each other (see Section 5.3.3). At the end of the test, the temperature of the shallow surface increases by  $19 - 29^{\circ}\text{F}$  and the temperature near the bottom of the borehole increases by  $22^{\circ}\text{F}$ , which is also roughly  $9^{\circ}\text{F}$  lower than inner DFOS data. The  $\Delta T$  in the supply and return pipes do not completely

converge below the depth of 250 ft but are very close. This indicates limited heat transfer between the looping pipe and the ground below this depth. The  $\Delta T$  below the depth of 310 ft is abnormal and unreliable.

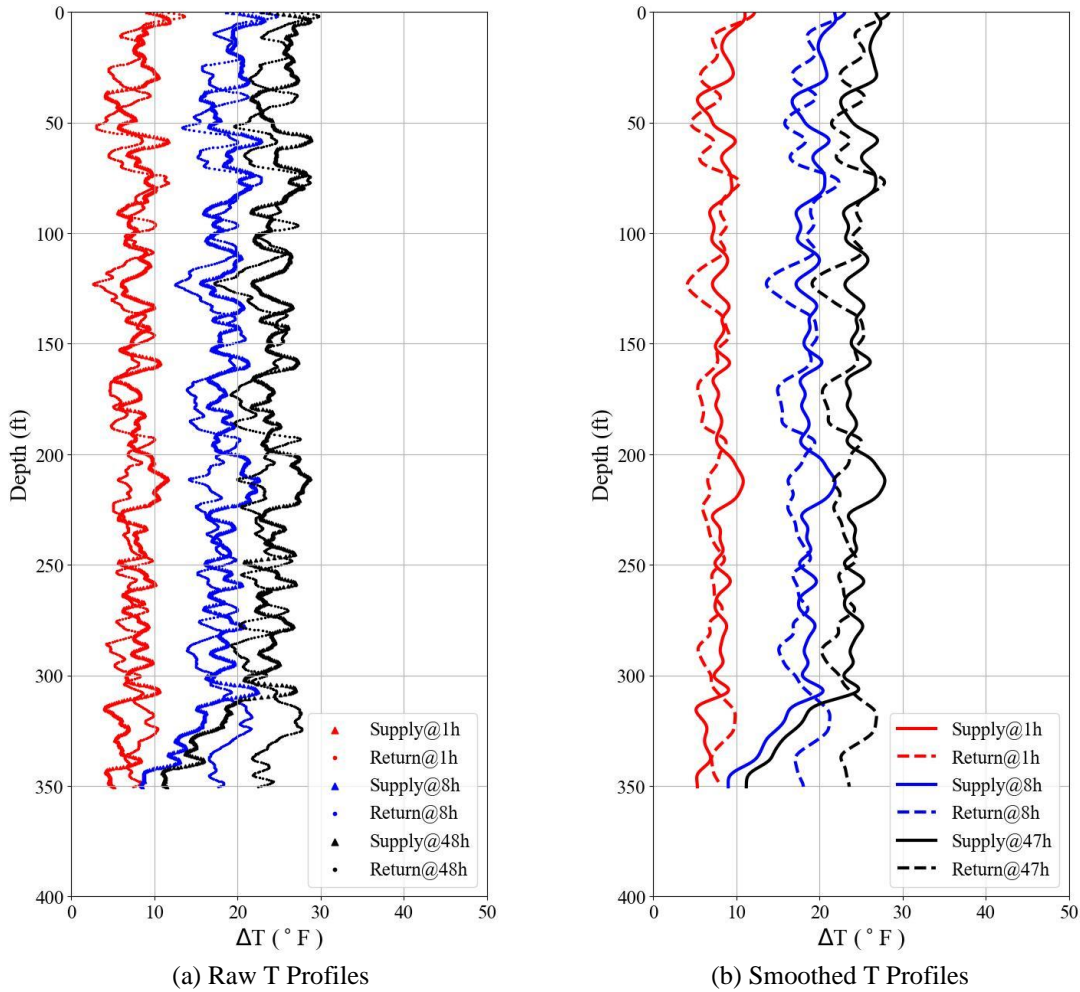


Figure 5.4.10 T vs. Elapsed at Different Times

## 5.5 Geothermal Properties

Thermal conductivity is usually calculated from the line source method, which assumes a constant heat input rate and ignores vertical heat transfer. This method is not appropriate for a TRT in layered ground conditions. To extract the vertical distribution of thermal conductivity from the DFOS data, the analytical method developed by McDaniel et al. (2018), following the work of Molz et al. (1989), is applied in this study. The method assumes the radial temperature gradients from the U-tube to the subsurface are constant and uniform at the steady state. The thermal conductivity values at different depths can be calculated from the temperature gradient and total average thermal conductivity when the test reaches a steady state. The equations used in the method are as follows:

$$\frac{\lambda_i}{\lambda_{ss}} = \frac{\frac{\Delta Q_{H,i}}{\Delta z_i}}{QP_H/B}$$

$$\Delta Q_{H,i} = \Delta T * Q_w * \rho_w * C_{p,w}$$

where  $\lambda_i$  is the thermal conductivity of  $i$ th layer;  $\lambda_{ss}$  is the total average thermal conductivity from traditional TRT;  $\Delta Q_{H,i}$  is the incremental heat flow;  $QP_H$  is the sum of  $\Delta Q_{H,i}$ ;  $\Delta z_i$  is the thickness of  $i$ th layer;  $B$  is the depth of the borehole;  $Q_w$  is the flow rate;  $\rho_w$  is the density of water, and  $C_{p,w}$  is the heat capacity of water. This equation can be reorganized as follows:

$$\lambda_i = \lambda_{ss} \left( \frac{T_{gradient,i}}{dT/B} \right)$$

where,  $T_{gradient,i}$  is the temperature gradient of the  $i$ th layer;  $dT$  is the temperature between the supply and return pipes at the surface.

The subsurface was divided into three main layers, and regression lines were used to represent  $\Delta T$  of the supply and return in each layer. Given that (i) there is an interface between sediment and bedrock at a depth of 30 ft and the analysis that (ii) the heat transfer efficiency below the depth of 250 ft is very low (see Sections 5.3 and 5.4), the tested ground is divided by the depth of 30 ft and 250 ft, and it is assumed that  $\Delta T$  below 250 ft is constant.  $\Delta T$  profiles at 46 hours and 47 hours are chosen as the steady state for the first and second tests, respectively. As discussed earlier, due to data fluctuation, the outer DFOS data is not used in calculating thermal conductivity.

Figures 5.5.1 and 5.5.2 show the simplified temperature profile, temperature gradient, and thermal conductivity of the first and second TRTs. In the first test,  $\lambda$  for the sediment above 30 ft is 6.2 Btu/hr-ft-°F, and  $\lambda$  for the bedrock from 30 ft to 250 ft is 1.4 Btu/hr-ft-°F; in the second test,  $\lambda$  for the sediment above 30 ft is 1.35 Btu/hr-ft-°F, and  $\lambda$  for the bedrock from 30 ft to 250 ft is 2.0 Btu/hr-ft-°F. These two sets of DTRT data give different estimates of  $\lambda$ , and in the first test,  $\lambda$  for the sediment above 30 ft is too high. This is because temperature fluctuation can easily affect thermal conductivity calculated from a temperature gradient. Compared with conventional TRT, DTRT estimates higher thermal conductivities for sediment and bedrock above 250 ft due to the zone below 250 ft where the heat transfer rate is low. Conventional TRT cannot consider such an effect, thus underestimating the thermal conductivity of the subsurface, especially for the sediment above the depth of 30 ft.

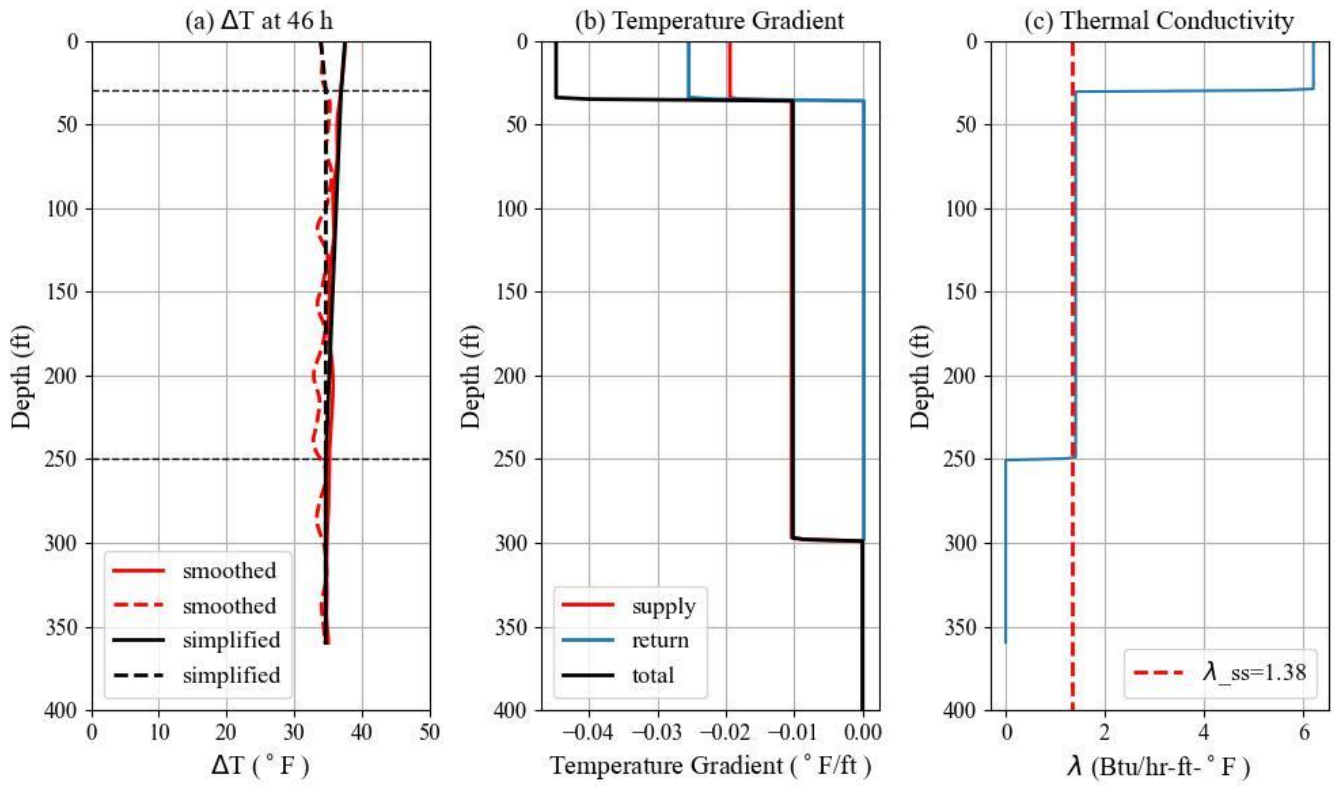


Figure 5.5.1 Thermal Conductivity of The First TRT

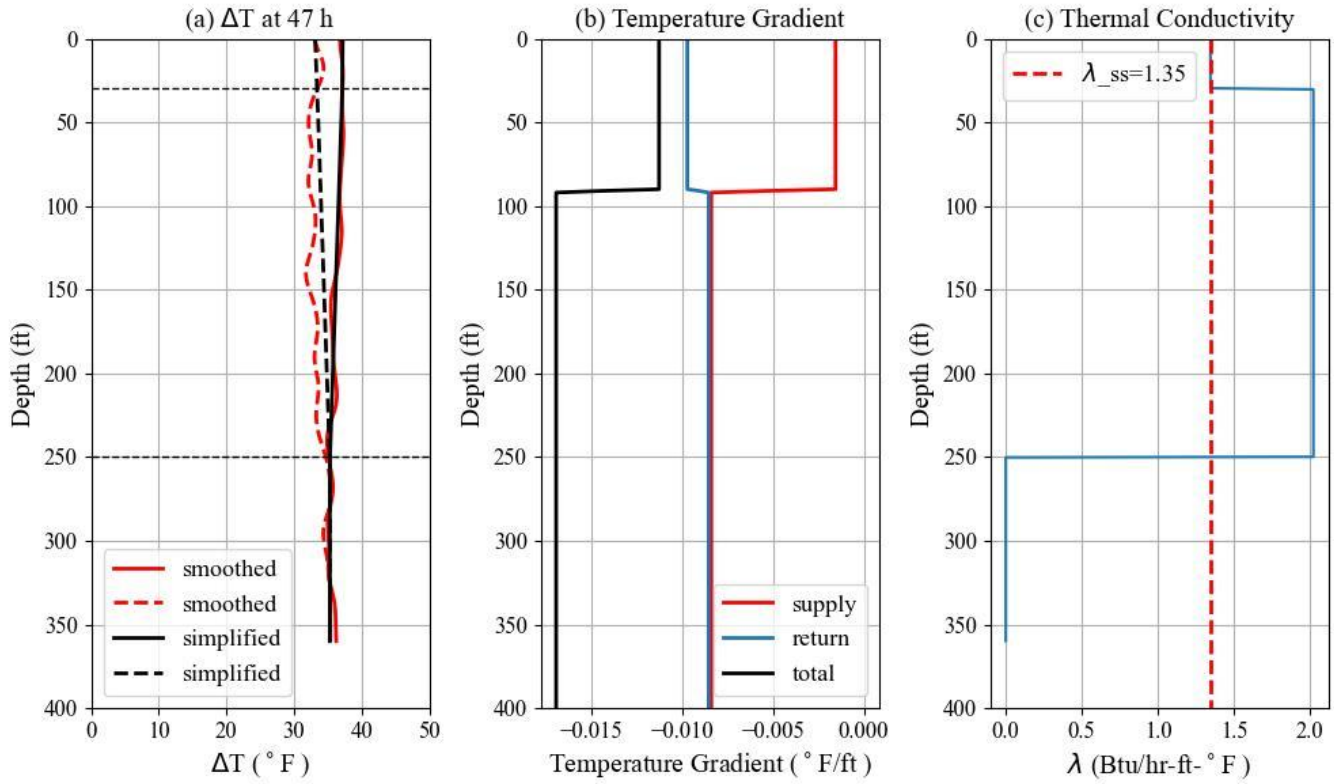


Figure 5.5.2 Thermal Conductivity of The Second TRT

The heat capacity profile at the test site is estimated based on typical heat capacity values of soils/rocks listed by Kavanaugh & Rafferty (2014). As shown in Table 5.5.1, the ground is divided into three layers, each with a range of heat capacity. By combining the heat capacity with the thermal conductivity profiles in the previous analysis, the thermal diffusivity profile is acquired and shown in figure 5.5.3. In the first DTRT, the thermal diffusivity of the sediment above 30 ft is  $3.5 - 7.5 \text{ ft}^2/\text{day}$ , and the thermal diffusivity of the bedrock from 30 ft to 250 ft is  $0.8 - 1.2 \text{ ft}^2/\text{day}$ ; in the second DTRT, the thermal diffusivity of the sediment above 30 ft is  $0.7 - 1.6 \text{ ft}^2/\text{day}$ , and the thermal diffusivity of the Franciscan Complex from 30 ft to 250 ft is  $1.1 - 1.8 \text{ ft}^2/\text{day}$ . As previously discussed, the difference is mainly caused by data fluctuation.

Table 5.5.1 Layered Heat Capacity

# Layer	Description	From (ft)	To (ft)	Heat Capacity (Btu/ft <sup>3</sup> ·°F)	
				Lower Bound	Upper Bound
1	Clay	0	10	20.0	41.5
2	Sandy gravel	10	30	20.2	43.0
3	Franciscan Complex	30	401	27.3	40.8

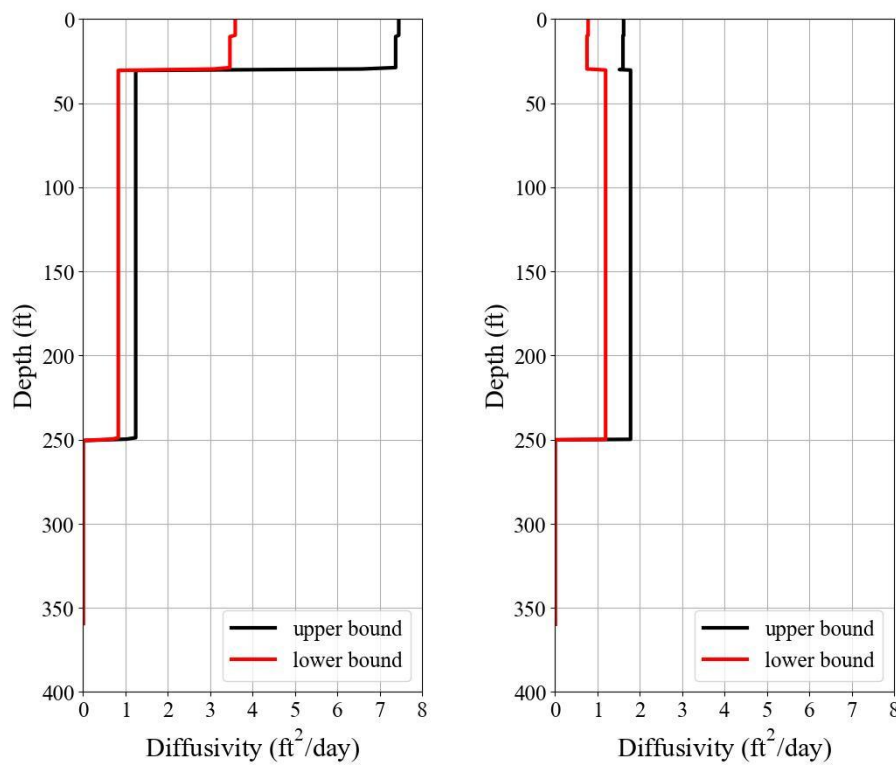


Figure 5.5.3 Thermal Diffusivity Profiles

## 6 Conclusion

This report describes the findings from the geothermal borehole investigation conducted at the UC Berkeley campus in the summer and autumn of 2022. It includes (i) the ground profiles from the borehole investigation and (ii) the geothermal properties derived from the two distributed thermal response tests. The main conclusions are summarized as follows:

1. The geological database of the UC Berkeley campus was established based on the existing geotechnical investigations. Combined with the geological background and in-situ boring study, the ground profile at the test site is divided into (i) fill (0 – 3 ft thick), (ii) upper clay layer (20 – 40 ft thick), (iii) clayey sand with gravel (5 – 10 ft thick) and (iv) Franciscan Complex (very thick). The Franciscan Complex, a mélange of sandstone (greywacke), shale, conglomerate, quartz, serpentinite, etc., and beneath the Berkeley campus, is primarily sandstone (greywacke) interbedded with shales. Sheared zones generated by tectonic activities can be found at depths of 75 ft, 200 ft, 280 ft, and 330 ft.
2. A borehole for TRT was drilled with multi-type geotechnical sensors installed. The geophysical logging shows that the borehole tilts less than 5° above the depth of 230 ft, and the tilt increases to 12 degrees at the bottom. This may affect the DTRT results, but there is no direct link between the tilt of the borehole and the anomaly in the DTRT results. The P-wave velocity profile can be divided into 2800 – 3350 ft/s (0 – 16 ft, sediment above water), 6000 – 8410 ft/s (18 – 23 ft, sediment below water), and 9000 – 18700 ft/s (below 24 ft, bedrock), whereas the S-wave velocity profile can be divided into 870 ft/s – 2570 ft/s (0 – 23 ft, sediment) and 3470 – 9380 ft/s (below 23 ft, bedrock). The geophysical logging identifies sheared zones at the depths of 75 ft, 170 ft, 200 ft, 240 ft, 280 ft, and 330 ft. It matches the boring log result and reveals more potential sheared zones.
3. Temperature monitoring before the TRT tests was performed using DFOS and Vibrating Wire Piezometer outside the pipe. The average geothermal gradient is 0.0136 °F/ft (24.79 °C/km) when the ground temperature is stabilized. DFOS performed well in monitoring the spatial and temporal variation of temperature during the grouting process. It revealed that the interruption of grouting when reaching the depth of 280 ft caused the anomaly in temperature reading below the depth of 280 ft, which affected the subsequent TRTs.
4. Two TRT were performed using the DFOS placed inside and outside the looping pipe. The DFOS performed well in analyzing the spatiotemporal variability of temperature change during the tests.

The inlet and outlet temperature data gave the effective thermal conductivities to be 1.38 Btu/hr-ft-°F (the first test) and 1.35 Btu/hr-ft-°F (the second test). In the heating phase, the temperature rise is linear to the natural log time; in the temperature decay phase, the temperature drop becomes slower after 20 hours; hence, the relationship is not linear to the natural log time. Heat transfer from the supply pipe to the return pipe can be observed.

5. Both temperature data from the DFOS inside and outside the looping pipe show some fluctuations along the depth. The main contributing factors are variations in geological conditions and grouting quality. Compared to the performance of the DFOS inside the looping pipe, the DFOS outside the pipe recorded a lower temperature, as expected. It could not measure the difference in the temperature profile between the inner and outer pipes observed in the inner pipe DFOS.
6. The thermal conductivity profile of the site was estimated from the simplified temperature gradient profile and the total average thermal conductivity. For the sediment (above 30 ft) and the bedrock (30 – 250 ft) in the first test, the thermal conductivity is 6.2 Btu/hr-ft-°F and 1.4 Btu/hr-ft-°F, respectively, and the thermal diffusivity is 3.5 – 7.5 ft<sup>2</sup>/day and 0.8 – 1.2 ft<sup>2</sup>/day, respectively; for the sediment (above 30 ft) and the bedrock (30 – 250 ft) in the second test, the thermal conductivity is 6.2 Btu/hr-ft-°F and 1.4 Btu/hr-ft-°F, respectively, and the thermal diffusivity is 0.7 – 1.6 ft<sup>2</sup>/day and 1.1 – 1.8 ft<sup>2</sup>/day, respectively. Both tests indicate the heat transfer efficiency of the ground below the depth of 250 ft is relatively low, with  $\lambda$  close to zero. This is related to the poor grouting quality below the depth of 250 ft.

## 7 Discussion and Future Works

Applying DFOS in thermal response tests allows the estimate of geothermal properties at different depths, and geothermal potential at the test site can be evaluated more accurately. However, the temperature profile measured by DFOS is very vulnerable and might suffer from spatial fluctuation along the depth. The main reasons include variable grouting quality and geological conditions. Besides, vibration and force generated by water circulation might change the stress state of the inner DFOS and cause data fluctuation, especially in the return pipe where the water might push up the DFOS. For the outer DFOS, the data quality will also be affected by the position of the sensor. Thus, to get an excellent temperature profile from DTTRT, installing DFOS is very important and should be improved in future projects.

In this report, the analytical model proposed by McDaniel et al. (2018) is used as a fast method to estimate profiles of geothermal properties. However, this method is susceptible to the spatial fluctuation of temperature along depth and gives unreasonable values at some depths. It assumes the radial temperature gradients from the U-tube to the subsurface are constant and uniform at the steady state, limiting the result. Limitation of assumption is also a common shortage in all analytical models. Hence, to better estimate geothermal properties, the finite element model will be run to match the temperature profiles from DTRTs, and geothermal properties will be evaluated through inverse analysis. The residual heat dissipation into the ground during the temperature decay phase will also be studied through the FE method.

## Reference

- Acuña, J. (2013). Distributed thermal response tests: New insights on U-pipe and Coaxial heat exchangers in groundwater-filled boreholes (Doctoral dissertation, KTH Royal Institute of Technology).
- Acuña, J., & Palm, B. (2013). Distributed thermal response tests on pipe-in-pipe borehole heat exchangers. *Applied Energy*, 109, 312-320.
- Beier, R. A., Fossa, M., & Morchio, S. (2021). Models of thermal response tests on deep coaxial borehole heat exchangers through multiple ground layers. *Applied Thermal Engineering*, 184, 116241.
- Beier, R. A., Morchio, S., & Fossa, M. (2022). Thermal response tests on deep boreholes through multiple ground layers. *Geothermics*, 101, 102371.
- Carslaw, H. S., & Jaeger, J. C. (1959). Conduction of heat in solids. Clarendon Press, Oxford, UK.  
Conduction of heat in solids. 2nd ed. Clarendon Press, Oxford, UK.
- Fujii, H., Okubo, H., Nishi, K., Itoi, R., Ohyama, K., & Shibata, K. (2009). An improved thermal response test for U-tube ground heat exchanger based on optical fiber thermometers. *Geothermics*, 38(4), 399-406.
- Gehlin, S. (2002). Thermal response test: method development and evaluation (Doctoral dissertation, Luleå tekniska universitet).
- Liu, J., Wang, F., Cai, W., Wang, Z., & Li, C. (2020). Numerical investigation on the effects of geological parameters and layered subsurface on the thermal performance of medium-deep borehole heat exchanger. *Renewable Energy*, 149, 384-399.
- McDaniel, A., Tinjum, J., Hart, D. J., Lin, Y. F., Stumpf, A., & Thomas, L. (2018). Distributed thermal response test to analyze thermal properties in heterogeneous lithology. *Geothermics*, 76, 116-124.
- Mogensen, P. (1983). Fluid to duct wall heat transfer in duct system heat storages. Document-Swedish Council for Building Research, (16), 652-657.
- Molz, F. J., Morin, R. H., Hess, A. E., Melville, J. G., & Güven, O. (1989). The impeller meter for measuring aquifer permeability variations: evaluation and comparison with other tests. *Water Resources Research*, 25(7), 1677-1683.

- Raymond, J., & Lamarche, L. (2013). Simulation of thermal response tests in a layered subsurface. *Applied energy*, 109, 293-301.
- Raymond, J., Therrien, R., Gosselin, L., & Lefebvre, R. (2011). Numerical analysis of thermal response tests with a groundwater flow and heat transfer model. *Renewable Energy*, 36(1), 315-324.
- Sakata, Y., Katsura, T., & Nagano, K. (2018). Multilayer-concept thermal response test: Measurement and analysis methodologies with a case study. *Geothermics*, 71, 178-186.
- Signorelli, S., Bassetti, S., Pahud, D., & Kohl, T. (2007). Numerical evaluation of thermal response tests. *Geothermics*, 36(2), 141-166.
- Silva, W., Wong, I. and Schneider, J., Earthquake scenario ground motion maps for the San Francisco bay region for a repeat of the M7.9, 1906 Earthquake.
- Trask, P. D., & Rolston, J. W. (1951). Engineering geology of san Francisco bay, California. *Geological Society of America Bulletin*, 62(9), 1079-1110.
- Zeng, S., Yan, Z., & Yang, J. (2022). Stepwise algorithm and new analytical model for estimating multi-parameter of energy piles from thermal response tests. *Energy and Buildings*, 256, 111775.
- Field, E.H., and 2014 Working Group on California Earthquake Probabilities, 2015, UCERF3: A new earthquake forecast for California's complex fault system: U.S. Geological Survey 2015–3009, 6 p., <https://dx.doi.org/10.3133/fs20153009>.
- Field, E. H., Biasi, G. P., Bird, P., Dawson, T. E., Felzer, K. R., Jackson, D. D., ... & Zeng, Y. (2015). Long-term time-dependent probabilities for the third Uniform California Earthquake Rupture Forecast (UCERF3). *Bulletin of the Seismological Society of America*, 105(2A), 511-543.
- Kavanaugh S. & Rafferty K. (2014). Geothermal Heating and Cooling: Design of Ground-Source Heat Pump Systems, Atlanta: ASHRAE, 75.

## **Appendix A**

### **Drilling Log**

# **Appendix B**

## **Boring Log**

# **Appendix C**

## **Geophysical Log**

## **Appendix D**

### **GRTI Report of 1<sup>st</sup> TRT**

## **Appendix E**

### **GRTI Report of 2<sup>nd</sup> TRT**